

Laser Powder Bed Fusion and Direct Laser Deposition of Metals and Alloys: A Review of Developments, Process Insights, and Ni-Based Superalloy Case Studies

**Amirhossein Riazi¹, Seyed Hossein Razavi^{1*}, Alireza Khavandi¹, Mostafa Amirjan²,
Mohsen Ostad Shabani³, Hossein Davarzani⁴, Yazdan Shajari³**

1. School of Metallurgy & Materials Engineering, Iran University of Science and Technology (IUST), Narmak, Tehran, Iran

2. Metallurgy Research Department, Niroo Research Institute (NRI), Tehran, Iran, 1468617151

3. Materials and Energy Research Center (MERC), Tehran, Iran

4. MAPNA GROUP, TUGA, Tehran, Iran

Abstract

Additive manufacturing (AM) of metallic parts has gained significant attention in recent years due to its ability to produce components without traditional tooling such as molds, melting furnaces, or extensive raw material preparation. Its unique capability to fabricate complex geometries has revolutionized part design and enabled substantial weight reduction. This review first outlines the development trajectory of metal-based AM, with a particular focus on laser-based fusion methods, including Laser Powder Bed Fusion (LPBF) and Direct Laser Deposition (DLD). Understanding this evolution helps researchers identify both the capabilities and limitations of AM technologies, thereby enhancing their application in areas such as prototyping, mass production, and repair. Each metal possesses unique physical and chemical properties, which often make traditional manufacturing methods more challenging—especially for alloys with high strength, hardness, or temperature resistance. In this context, the review then focuses on nickel-based superalloys (NBSAs), which are widely used in high-temperature and high-stress environments but are particularly difficult to process using conventional techniques. Their application serves as a representative case study for evaluating the performance and feasibility of AM techniques for advanced materials. Furthermore, the future prospects of AM are discussed, including advancements in monitoring systems, integration of machine learning, and the development of AM-specific alloys. As a novel aspect, this work compares LPBF and DLD in terms of their advantages, limitations, and resulting material properties, along with a comparison to traditional manufacturing methods such as casting and wrought processing.

Keywords: Additive manufacturing, Nickel-based superalloys, Laser Powder Bed Fusion, Direct Laser Deposition, advanced materials

Contents

I. Introduction	5
II. Types of Processes.....	8
1. Laser Powder Bed Fusion (LPBF).....	9
1.1. Selective Laser Melting (SLM).....	9
1.2. Selective Laser Sintering (SLS)	11
1.3. Direct Metal Laser Sintering (DMLS)/Direct SLS	12
1.4. Comparison Between LPBF and SLS	13
2. Flow-based or Directed Energy Deposition (DED)	13
2.1. Direct Laser Deposition (DLD) Equipment and Process	14
3. Influence of Process Parameters and Scan Strategy on Microstructure and Properties	15
4. Comparison Between LPBF and DED	18
4.1. Advantages of DED / DLD Over LPBF.....	18
4.2. Disadvantages of DLD Compared to Powder-Bed	19
4.3. Powder-Bed Advantages Over Flow-Based Methods.....	19
4.4. Limitations of LPBF/Powder Bed Compared to DLD.....	19
5. Monitoring	20
5.1. Powder Bed Fusion Process Monitoring.....	20
5.2. Monitoring of Flow-Based Processes	21
6. Machine Learning.....	22
III. Mechanical properties.....	24
1. Various Items Influencing the Final AM-Developed Part's Quality	24
2. Different Types of Powders in the Additive Manufacturing Processes	25
3. Comparison Between Additive Manufacturing and Conventional Methods.....	27
3.1. Comparison Between Properties of AM and Conventional Methods	28
3.2. Impact of Build Direction on the Mechanical Properties.....	30
4. Scan Strategy Effect on the Mechanical Properties.....	34
4.1. Decrement of Residual Stress Using the Island Pattern	37
4.2. Hatch Spacing Distance	38
5. Defects (Pores and Cracks).....	39
5.1. Cracks.....	39
5.2. Pores	41

6. A Commentary on Additive Manufacturing of Gamma-Prime Inducing NBSAs.....	46
7. Microscopy	47
8. Applicable Mechanical Tests.....	48
9. Improvement of AM-Developed Part Properties by HIP Treatment.....	48
10. Advantages of Segregation Reduction and Homogeneity Enhancement in AM.....	49
11. New Materials	49
IV. Conclusion	51

In Press

I. Introduction

Additive manufacturing is one of the advanced production methods, considered one of the precursors of the fourth industrial revolution. This type of production has already replaced many traditional methods [1, 2]. All kinds of polymer, metal, and ceramic parts can be produced using AM. In the industry, several production methods could be used simultaneously to produce a piece. For instance, to produce a metal part by precision casting method, a polymer model of the part must be carved first. Then, molding is carried out using ceramic materials, and after producing molten steel, the casting process is completed, and finally, machining is performed. However, in the AM, only a computerized design file of the part and an additive manufacturing machine are needed. After receiving the file, the machine considers the design as a large number of layers stacked on top of each other and then starts to make the part [3-13].

Metals are widely used engineering materials that play a key role in industries. Traditional methods of producing metal parts, such as casting, shaping, and assembly, require equipment, tools, and high costs; however, additive manufacturing greatly simplifies the manufacturing process and, in many cases, provides higher-quality parts. On the other hand, by eliminating the complexities of production, the design of parts can be optimized. Therefore, in cases such as aviation applications where the weight of parts is important, lighter parts can be produced with higher efficiency [14].

The function of additive manufacturing machines is that parts are produced by joining raw materials together. In order to join metallic materials together, with the radiation of an energy source, the particles are partially or completely melted and added to the previous ones. After passing the energy beam, the melted part immediately solidifies. The energy beam is mainly created by the source of a laser beam or electron beam. Due to the easier accessibility and use of

lasers, this energy source has become more widespread in additive manufacturing machines. The laser beam provides a clean and reliable energy source for the fabrication of metallic parts. The additive manufacturing performed using a laser energy source is named laser-based additive manufacturing (LBAM) [15-19]. LBAM offers a key advantage over electron beam methods: it can operate in an inert gas atmosphere, making it more practical and widely applicable in industrial environments. In contrast, other sources such as arc-based systems lack sufficient controllability during processing and generate a large heat-affected zone (HAZ), which can introduce defects [20, 21]. The laser source, with its small spot size, enables precise and controlled energy input, making it suitable for both manufacturing and repair processes.

Traditionally, repair of worn components was performed using welding techniques such as Tungsten Inert Gas (TIG) welding. However, these methods often create large melt pools that compromise substrate properties and induce defects like pores and cracks [22]. The evolution of AM technologies, particularly LBAM, has introduced a more reliable and controllable alternative for defect-free fabrication and repair of parts [23].

For instance, turbine components must meet strict quality standards to operate in extreme environments, and in recent years, many of these parts have been successfully produced using LBAM. This method requires only a CAD model to fabricate complex geometries, eliminating the need for traditional manufacturing tools such as expensive casting molds or forging dies. Moreover, part designs have been customized and optimized for weight reduction in aerospace applications.

Another key benefit of LBAM is its ability to integrate component production, replacing traditional assemblies made of multiple joined parts with a single, consolidated structure. Today, LBAM is used across various industries, including automotive, defense, aerospace, and energy. In the harsh

environment of turbine operation, critical components of the combustion chamber—such as swirlers [24], inserts, and sleeves—are now manufactured using LBAM. The success of this technology has extended to the production of blades, vanes [25], and dampers in gas turbines.

Overall, LBAM offers substantial industrial advantages by reducing raw material consumption, minimizing the number of parts and machining steps, and enhancing design flexibility. Notable applications include burner tips, fuel nozzles, and components in rocket engines and small aircraft engines [26-29].

The LBAM of metallic parts has attracted much attention from industrialists recently. This approach to LBAM is due to the advantages of this method over traditional methods. Some of the advantages and features of this method are as follows.

- Due to the high temperature of the melt pool, it is possible to make parts from difficult-to-machine and refractory materials.
- The layer-by-layer manufacturing process allows any complex geometric design to be produced without limitations.
- It is possible to produce parts by changing the raw material, and the microstructure of metals can be tailored. For instance, it is possible to produce nickel-based parts with a crystallized microstructure in a specific direction, $\langle 001 \rangle$.
- The properties of the produced parts are uniform throughout the whole part, and common defects, such as coring and segregation, are not observed in them.
- High energy density and small HAZ, which leads to a decrease in grain size, and therefore, an increase in the part's mechanical properties.
- Unlike casting and wrought methods, additive manufacturing does not require different equipment and molds for each new sample and has the highest speed and lowest cost for

custom production. Therefore, additive manufacturing is currently the best option in industries, such as aviation and biomaterials, where the variety of shapes of parts is high and the number of production is small [30-35].

In other reviews, the details of AM methods for various alloys, such as NBSAs, have been thoroughly covered [36-38]. However, understanding the development process of AM methods and how they have evolved to their current state can provide deeper insights into the advantages, disadvantages, capabilities, and limitations of each method. This review was conducted with this perspective in mind, aiming to help readers make informed decisions when selecting the appropriate AM method based on the desired final quality. For instance, using powder bed methods instead of flow-based ones might result in higher-quality parts. Conversely, understanding the limitations of the powder bed method could encourage leveraging the capabilities of flow-based methods to produce integrated parts with higher production rates.

II. Types of Processes

The LBAM of metallic parts can be categorized into three main types: powder-bed fusion (PBF), flow-based or directed energy deposition, and sheet lamination. Figure 1 illustrates a specific classification of LBAM systems used for metals.

The LBAM techniques employ various materials, such as powder, wire, and sheet. While powder-bed-based systems exclusively use powder, flow-based systems can utilize either powder or wire [15, 35]. Sheet lamination techniques solely rely on the use of sheets [35]. This review explains the two most common methods, powder-bed and flow-based. The sheet lamination has no usage in the industry; therefore, this method was not addressed in this review.

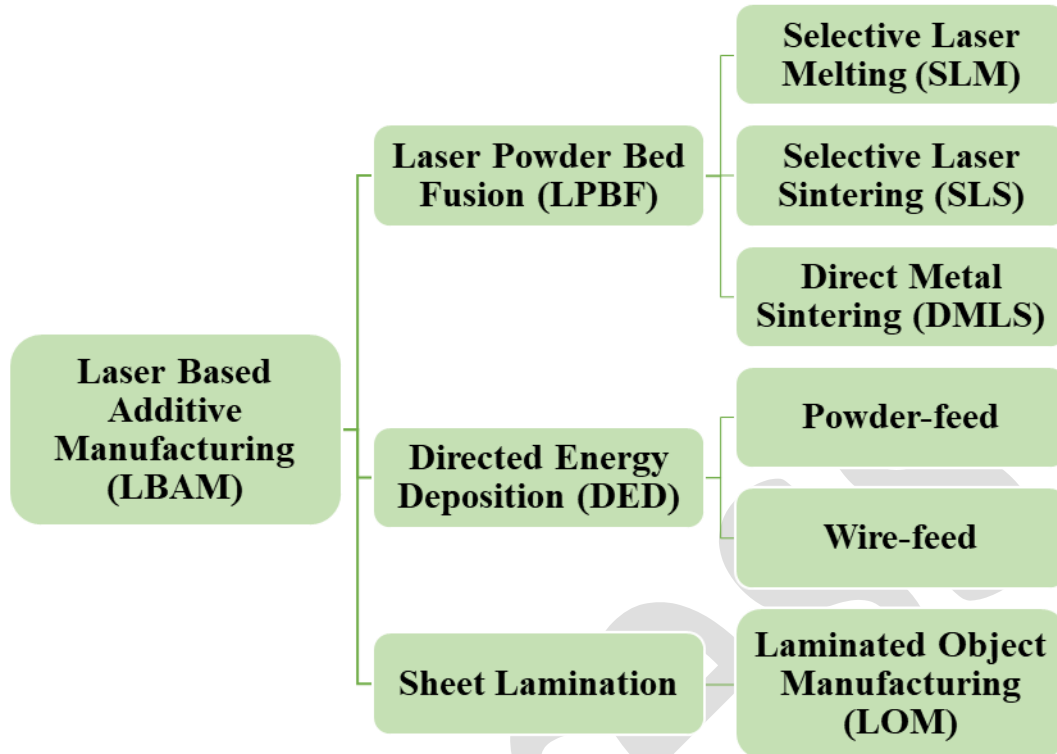


Fig. 1. Classification of LBAM techniques for metallic materials [35]

1. Laser Powder Bed Fusion (LPBF)

The LPBF is a subgroup of LBAM that utilizes a high-energy laser source to selectively melt or sinter a metallic powder bed [39, 40]. The LPBF methods can be further divided into three categories, briefly described in Sections 1.1 to 1.3.

1.1. Selective Laser Melting (SLM)

The SLM technique demonstrates the capacity to produce components with considerable material density, precise dimensional integrity, and desired mechanical properties. Within the SLM process, successive layers of metallic powder undergo fusion and consolidation, culminating in the development of intricate three-dimensional structures [28]. The SLM enables the fabrication of complicated components with nearly 100% density, thereby ensuring uniform characteristics across a series, obviating the need for subsequent post-processing stages [1, 11, 35].

The SLM technique provides the most typical features of powder-based additive manufacturing because of its flexibility in feedstock and shapes. Both inert argon and nitrogen gas can be utilized in the SLM process. The schematically working system of the SLM machine is demonstrated in Figure 2. Nowadays, SLM terminology is mainly known as its group head, LPBF; therefore, in the case of this review, it will be regarded. Refer to ASTM 52900-2022 for more details about additive manufacturing terminologies.

Despite the numerous advantages of LPBF, it still exhibits certain limitations in its processing compared to traditional manufacturing techniques. Due to the localized concentration of energy input, a temperature gradient mechanism is induced, resulting in plastification and subsequent generation of residual stress, ultimately leading to deformation. These residual stresses play a pivotal role in affecting dimensional accuracy and propagation of cracks, potentially causing detachment of parts from the base plate [41].

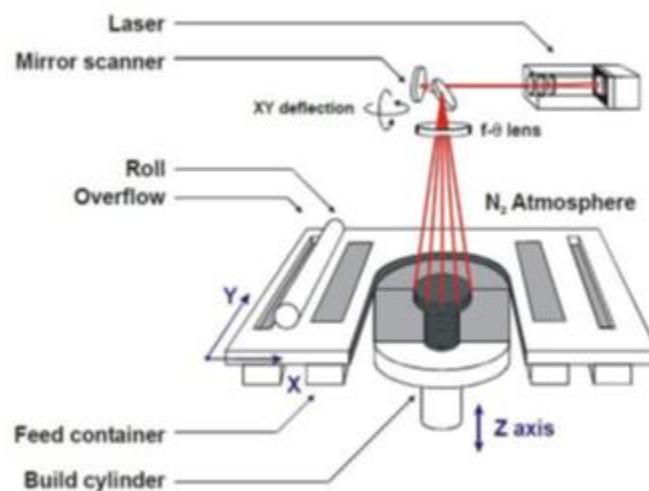


Fig. 2. Schematic representation of an SLM machine [1]

It would be suggested that the material be preheated to minimize the residual stress. The normal thickness of the layers in the LPBF process is between 20 to 100 μm . In the process, one of the Nd: YAG or CO_2 lasers is used as the heat source. A wide range of metallic materials can be processed by the LPBF. Some of these materials are as follows: stainless steel, aluminum, copper, iron, cobalt-chrome, titanium, NBSA, and a mixture of mentioned ones [35, 42].

1.2. Selective Laser Sintering (SLS)

In the SLS process, a mix of two different powders is used. One powder is structural, and the other is sacrificial as a binder. The SLS machine works similarly to the LPBF, and the powder is different. The structural powder is a metallic material, and the sacrificial powder is a polymer. While the laser beam irradiates the powder mixture, only the polymer melts, and the structural powder remains unchanged. The fused polymer binds the structural material together and makes an integrated part. Heat treatment should be applied to remove the binder and sinter the structural powder. Thereby, the sintered part, known as the green part, is held in order of 900°C temperature. The green part has approximately 50% porosity [35]; as a result, the sintered component undergoes a transformation process through infiltration with a low melting point metal or alloy, such as copper, brass, and bronze, thereby yielding a dense composite alloy component [43]. It is noteworthy that the accuracy of the SLS process is challenging to predict as it is a function of various parameters, some of which can be mutually dependent. The parameters that have the most influence on SLS/Rapid Prototyping accuracy can be divided into three groups: pre-processing, processing, and post-processing errors [44]. Mostly, the layer thickness is between 100 to 300 μm , and SLS resolution is also in the order of 100 μm . One of the advantages of SLS is the lower consumption of energy. Therefore, the embedded laser can be each fiber, CO_2 , or disc laser without any specific limitation. Furthermore, the other advantage is the processing possibility of a wide

range of materials, such as sand, stainless steel, and different plastics [35]. Metal powders find their exceptional applicability in the realm of SLS, as it is challenging to directly fabricate metallic components using alternative rapid prototyping, rapid tooling, or rapid manufacturing (RP/RT/RM) methods [45].

The SLS can be further enhanced through a variation known as SLS/Hot Isostatic Pressing (SLS/HIP), which introduces several advantageous features into the manufacturing process. The SLS/HIP represents a net-shape manufacturing approach that merges the inherent freeform shaping capabilities of SLS with the complete densification potential of HIP [43]. These two features are next to each other, leading to a reduction in manufacturing costs. In the mere SLS, the part has a densification of approximately 80%. After HIP treatment, a fully dense specimen can be produced. The HIP process uses an inert gas like argon, and the put sample experiences a high temperature at a high level of isostatic pressure. The details of the method, such as layer thickness and the resolution, are the same as mentioned about SLS [35]. According to Liu et al. [43], cold isostatic pressing exerts a nearly equivalent influence on the final properties of the component. This method is particularly suited for processing durable, high-strength materials like IN625 and Ti6Al4V [35].

1.3. Direct Metal Laser Sintering (DMLS)/Direct SLS

The technique known as DMLS or Direct SLS involves the utilization of two distinct types of metal powders. One of these powders possesses a high melting point, serving as the structural metal, while the other features a lower melting point, fulfilling the role of a binder [33]. It is noteworthy that the DMLS process can alternatively employ a single powder with varying grain sizes, where the powder with a smaller size is fused, and coarse/structural powder will sit in it [35].

In its fundamental concept, the DMLS process closely resembles SLS. However, DMLS employs uncoated pre-alloyed metal powders as raw material, whereas SLS relies on polymers or coated metal powders [4].

Both the SLS and DMLS are suitable for tooling; DMLS does not need the time-consuming step of removing excessive binder material. This advantage makes the production process faster and more economical. Therefore, the DMLS method can be applied to produce prototype models, molds, and dies [44, 46].

1.4. Comparison Between LPBF and SLS

In the LPBF process, the powder completely melts during the laser beam irradiation. This full melting manufactures a final part with high density, and its quality is comparable to that of the conventional method. The SLS parts have a high porosity volume; thereby, their final quality is decreased [35, 44, 47].

Melt infiltration and removal of the binder are two time-consuming steps. The LPBF parts do not need any specific post-processing. Therefore, if the surface roughness is ignored, the final part after the cutting from the substrate can be used in industrial applications [35, 44, 47].

Therefore, in the past few years, LBAM of metallic materials has been considered limited to LPBF and directed energy deposition (DED) processes and no longer pointed to SLS [2, 48, 49]. Moreover, in the continuation of this review, only LPBF properties are reported, and SLS reports are ignored as much as possible.

2. Flow-based or Directed Energy Deposition (DED)

The flow-based deposition is based on the injection of the powder or a wire as the feeder of the process to create a metallic part. The injected wire or powder melts by a heat source. Moreover, a

laser or an electron beam can be used as the heat source. The process is called "directed energy deposition (DED)" or "direct metal deposition." If the heat source is a laser, the process is also known as "directed laser deposition" [2, 39, 50]. Due to the numerous brands that produced the DED machine, the process has taken many names. Some of the most prevalent ones are laser-engineered net shaping (LENS) [50], direct light fabrication (DLF) [51], laser consolidation (LC) [52], laser rapid forming (LRF) [53], and laser cladding (often for coatings) [35].

2.1. Direct Laser Deposition (DLD) Equipment and Process

The DLD mechanism consists of the blown powder or injected wire that is introduced to a substrate and melts by a focused laser while reaching (Figure 3). The laser type is a high-power one and can be gas-CO₂ or fiber-Nd: YAG. In some handy-made DLDs, a CNC with a powered laser and a powder blower pump can form the machine [51-53].

Blowing of the powder or injecting the wire is carried out by a nozzle. In order to prevent the oxidation of the created melt atop the substrate, an inert gas is blown into the melt pool. Moreover, in the powder DLD process, the volume of blown powder is often several times more than what melts, i.e., a large volume of the powder blown from the nozzle remains unscraped and unused and just plays the role of the oxidation barrier. Furthermore, the inert gas for the powder-base DLD and the oxidation barrier play the role of the powder carrier [53, 54].

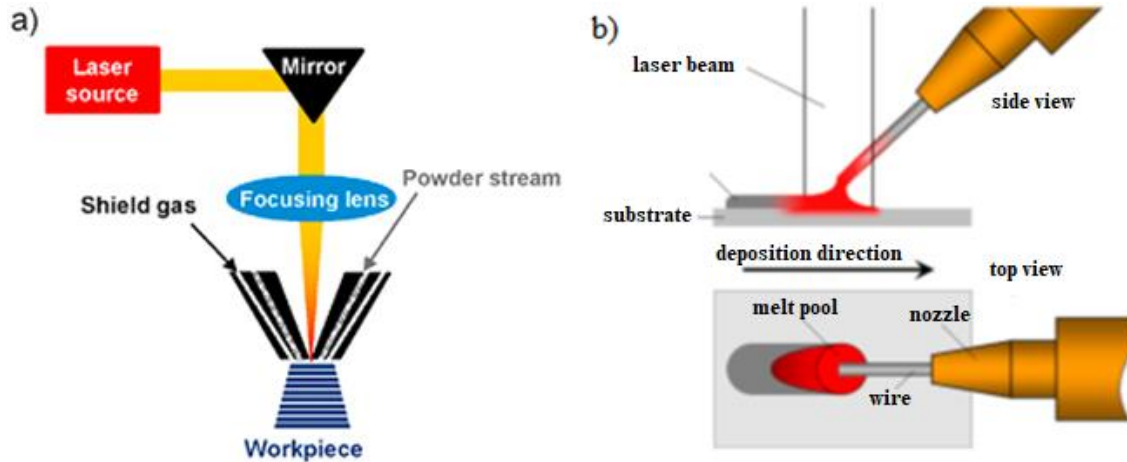


Fig. 3. Schematic drawing of the DLD process, a. powder-feed laser deposition, and b. Wire-feed laser deposition [51, 52]

3. Influence of Process Parameters and Scan Strategy on Microstructure and Properties

Process parameters significantly influence the microstructure and mechanical properties of the part. These parameters can be broadly categorized into two main groups: those affecting (1) energy density and (2) layer thickness [5, 55-58]. Any critical factor impacting part quality may be considered a process parameter, including laser source characteristics, part design, machine components (e.g., nozzle configuration), and raw material properties.

In the DLD method, the most critical process parameters are generally grouped into four main categories: laser power, laser scanning velocity, powder mass flow rate [59, 60], and hatch spacing [35, 61]. With the exception of powder mass flow rate, these parameters are also relevant in the LPBF process. However, in LPBF, the layer thickness is a key parameter that replaces the powder mass flow rate used in DLD. It is important to note that LBAM processes may include additional process parameters—for instance, laser beam focus diameter and laser standoff distance, both of which can influence build quality in DLD and LPBF methods [62].

Moreover, scan strategy or pattern is another influential factor that affects the properties of the final part (Figure 4). Various scan strategies—such as unidirectional, bidirectional, continuous, and raster/island—result in distinct material properties [63]. In certain cases, interlayer rotation is essential for achieving a dense, pore-free structure. For example, in one study (Table 1), a 30° interlayer rotation increased the density of Inconel 718 parts from 8.11 to 8.20 g/cm³ [62]. Parts produced with interlayer rotation typically exhibit a basket-weave structure, as illustrated in Figure 9 [35]. Further discussion on scan strategies is provided in Section III.4.

Also, powder characteristics are closely linked to process parameter optimization. Selecting suitable parameters requires consideration of material properties. Attributes such as powder shape, size, and distribution directly influence process behavior, including flowability (especially in DLD), laser absorption, and surface morphology [47, 64, 65].

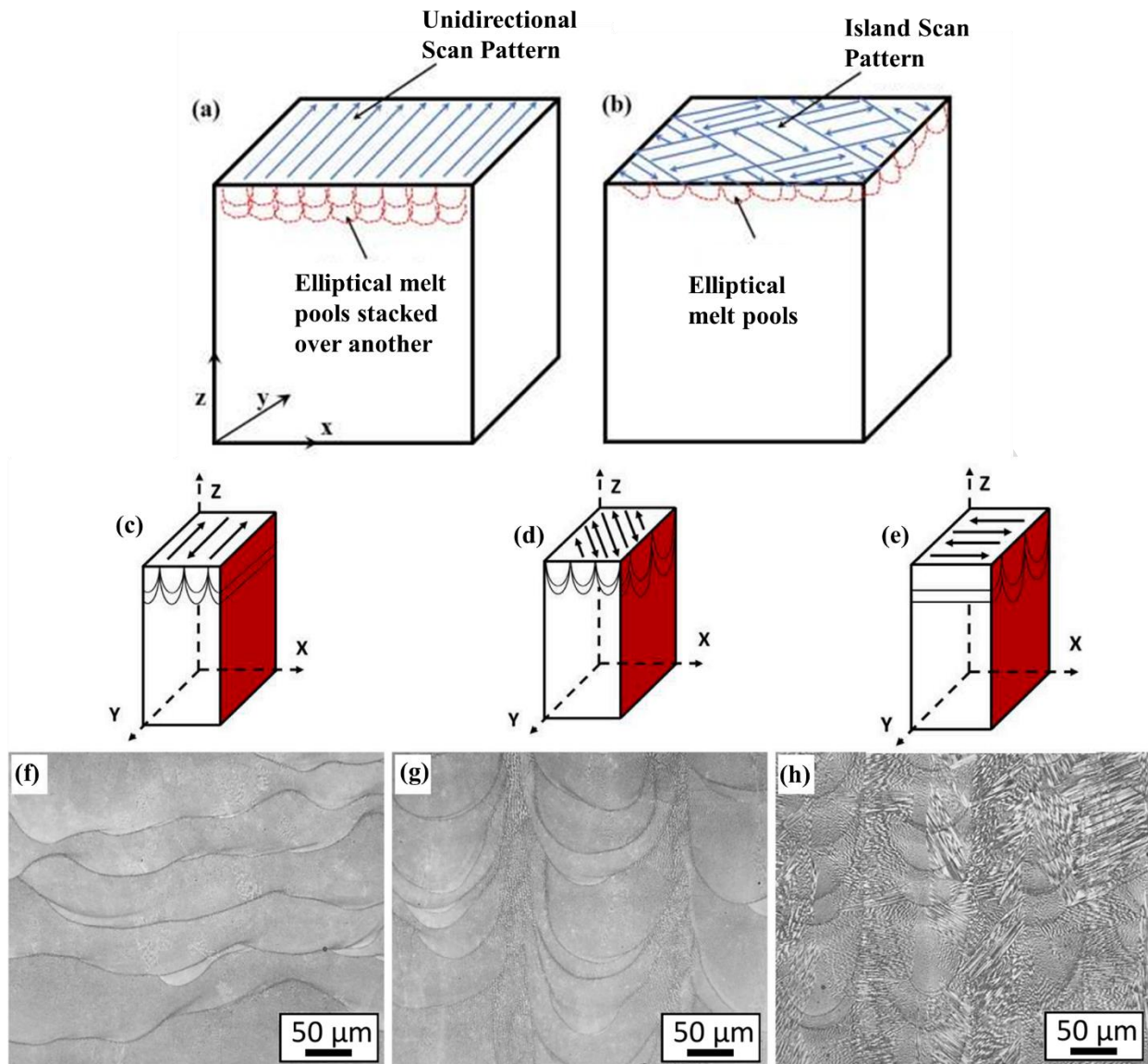


Fig. 4. Effect of scanning pattern on melt pool and microstructure: unidirectional (a) and island (b) scan patterns [66]; melt pool indications influenced by scanning orientation, interlayer rotation of 67 degrees (c to h) [67]

Table 1. Effect of interlayer rotation on increasing the density of the part/sample [62]

Interlayer rotation degree	Porosity (%)	Density (g/cm ³)
0	0.21	8.11
30	0.10	8.20

4. Comparison Between LPBF and DED

Each LPBF and DLD is used when considering the final required properties. The production speed of DLD is often higher than that of LPBF, and the surface quality of LPBF is better than that of DLD. Altogether, DLD may be offered for large parts in which the surface quality is not a limitation, and the production speed is important.

4.1. Advantages of DED / DLD Over LPBF

One of the most important advantages of DLD is its high productivity speed. The deposition rate is approximately 100 gr/h. The layer thickness reaches 250 μm , but the value for LPBF is conventionally less than 40 μm [35].

The other advantage is its freedom in the part size, which means that the DLD, as opposed to LPBF, is not constrained to the build chamber and powder container [35]. The other unique feature of DLD is the capability to produce functionally graded materials and a single material. Moreover, DLD can be used in repairing parts, often known as laser cladding repair [49, 54, 68-70].

4.2. Disadvantages of DLD Compared to Powder-Bed

The main disadvantage of the DLD process is the degraded surface quality. In DLD, the roughness is high and at least ten times higher than that of LPBF. Therefore, the final part must frequently be machined and surface treated [2, 35, 48].

Some defect formations are prevalent in DLD, which are as the following:

- Cracking and distortion initiated from a high cooling rate
- The porosity derived from the powder contamination and the gas entrapment
- Lack of fusion (LOF) and weak bonding between the layers
- Hatch line defects owing to improper process planning

4.3. Powder-Bed Advantages Over Flow-Based Methods

In powder bed processes like LPBF, the powder bed prevents the melt from falling. Accordingly, for parts having overhangs, LPBF is better than DLD. The other advantage of LPBF is its low residual stress. Altogether, thermal tension in the additive manufacturing processes is high because of fast repeated melting and cooling cycles. Nevertheless, this residual stress in LPBF is less than DLD because the powder bed inhibits the fast cooling of the melt section and exit of the heat [2].

Better surface quality and higher dimensional accuracy are the other basic advantages of LPBF over DLD. The purpose of applying additive manufacturing is to produce delicate parts with complex geometries. Therefore, owing to LPBF's superiority, it will be advised when high accuracy is required [71, 72].

4.4. Limitations of LPBF/Powder Bed Compared to DLD

Powder bed methods are constrained to the build chamber. However, in DLD, the process can be designed so that the part size can vary freely. The deposition rate of LPBF is lower than that of

DLD; nevertheless, it is noteworthy that in new LPBF machines, the total deposition rate has increased with the increase in the number of lasers. For instance, there are simultaneously 12 active lasers in some new LPBF machines [35, 47, 48, 73]. The LPBF process is more sensitive to the size of the powder. If the powder particles are large, the accuracy is challenged. If the powder is fine, the tendency to agglomeration increases and the flowability faces difficulty [47].

5. Monitoring

In past years, monitoring has been seriously discussed to find the onset of the defects in the serial production of the parts. In additive manufacturing processes, the stability and repeatability of the procedure are challenges. Some devices and software were designed to detect anomalies during the process quickly. The conventional tools to help the monitoring and detection of the distorted part are as follows [35, 64, 72, 74-79].

- Infrared (IR) imaging
- Ultraviolet (UV) imaging
- X-ray imaging
- Charge-coupled device (CCD) video imaging
- Photodiode
- Pyrometer
- Ultrasonic wave generator
- Complementary metal oxide semiconductor (CMOS) camera

5.1. Powder Bed Fusion Process Monitoring

In the PBF, the melt pool, the layer of the powder bed, the manufactured slice, and the under-scanning tracks can be evaluated. Another important issue in powder bed monitoring is the

spattering of the powder or melt. Since 2011, galvanic scanners have helped monitor the powder bed. The detection is based on measuring two angles and the wavelength differences resulting from the instant temperature. The detection normally faces displacement problems, which can be solved using two-dimensional sensors [75, 79-85]. Currently, most new monitoring systems are based on non-contact systems consisting of optical, thermal, and acoustic detectors. The mentioned devices and the rained computers powerfully detect the anomalies [64, 77].

5.2. Monitoring of Flow-Based Processes

The DLD process monitoring can be carried out in every step of powder delivery, melt pool, and layering.

- **Monitoring of Powder Delivery Rate**

A photodiode is set to measure the volume of the powder exiting from the nozzle. The more powder particles pass through the nozzle, the less light reaches the photoelectric sensor. Furthermore, the optical and acoustic sensors are promising measurement devices in the delivery rate step [30, 35, 78, 86, 87].

- **Monitoring of Melt Pool and Layer Morphology**

Melt pool monitoring is often based on thermal manners. A pyrometer and an IR sensor coupled with a CMOS or CCD camera can evaluate the melt pool morphology. Proper monitoring of the melt pool can evaluate and improve the geometrical integrity, as well as the microstructural and mechanical properties of the under-manufacturing part. Since the melt pool shrinks, lengthens, and splashes, its morphology during the laser scan is completely unstable. This instability makes it difficult to evaluate and monitor the process. In order to monitor the unsteady melt pool, thermophysical equations like Rothensal's analytical solution are mainly applied. Overall, melt

pool characteristics, such as peak temperature, length along a certain axis, and total area, are some of the process signatures [2, 35, 88, 89].

X-ray tomography is proposed as a new and reliable method to monitor layer morphology. The X-ray setup characterizes, quantifies, and identifies the layer morphologies and anomalies [90].

6. Machine Learning

Computers can help to detect anomalies in each step of the manufacturing process. This type of computer assistance is known as machine learning (ML). In some cases, ML is coupled with monitoring tools to detect and obviate process defects. There are many toolsets accessible for employment in the realm of image processing within the domain of ML, encompassing both freely available and commercially licensed alternatives. Noteworthy examples include the MATLAB Computer Vision Toolbox and the C++/Python OpenCV libraries. Overall, ML can improve all steps of the manufacturing process, from parameter settings to quality control. Numerous sciences like metallurgy, electronics, physics, and mechanics are engaged in additive manufacturing technology. Moreover, in each field of the process, many parameters and variables may change [91-95].

In order to optimize an additive manufacturing process, the computer takes the variation range of the parameters and assumes a step for each parameter/item, then compares the results and suggests the best one. For example, in one additive manufacturing process, the parameters and steps are according to Table 2.

Therefore, there are many degrees of freedom in normal additive manufacturing work. The computer considers all these degrees and offers the optimized one in supervised or unsupervised situations [96-100]

Table 2. Case study illustrating a method to optimize the process using design of experiments

Parameter/Item	Range/states	Step size	Number of states = (range size /step size) + 1
Power	100-300 w	20 w	11
Scan speed	500-1500 mm/s	100 mm/s	11
Hatch Distance	30-80 μm	10 μm	6
Layer Thickness	20-60 μm	10 μm	5
Next Layer Rotation	0-90 degrees	15 degrees	7
Amount of Recycled Powder	0-100 percent	20 percent	5
Build direction	0-90 degrees	15 degrees	7
Powder Size	15-53 μm / 60-80 μm	-	2
Scan strategy	Island/Regular Back-and-Forth	-	2

III. Mechanical properties

The mechanical properties of NBSAs have been investigated for several decades. Conventionally, the superalloy specimens were produced by wrought or casting. However, after the emergence of AM, it turned into a desired method. The additive manufacturing can produce refractory materials with high-temperature applications and manufacture parts in complex shapes.

Gas-turbine blades have both specifics, complicated designs, and high-temperature materials. The blades sometimes have air paths that make their design more complicated and harder to produce. Therefore, additive manufacturing seems to be a suitable method of manufacturing these parts, which has been investigated seriously in past years [101-105].

1. Various Items Influencing the Final AM-Developed Part's Quality

An extensive range of different parameters influences the properties of NBSAs. On the other hand, a wide variety of elements are used in the composition; this difference in the alloying makes the final properties more complicated. Therefore, AM-developed nickel-based parts need to optimize the process parameters, based on the added alloying elements. In the past years, much research has been dedicated to the metal additive manufacturing field, but it is not sufficient yet due to the variety of parameters, specifically for nickel.

- a. Process parameters of additive manufacturing significantly affect the specimen properties. The important parameters are scan velocity, laser power, hatch distance, and layer thicknesses [39, 106-108].
- b. The grain structure in NBSAs has an important impact on the part application. For high-temperature usage, mostly single crystal and columnar grains are used. In AM-developed parts, the structure prefers to form columnar dendrites. When the process parameters are

fixed, an equiaxed, columnar, or single-crystal structure can be determined. Some process conditions, such as build direction, preheat temperature of powder or substrate, and scan strategy, can help better tailor the desired dendrite structure [36, 37, 109-114].

2. Different Types of Powders in the Additive Manufacturing Processes

Since additive manufacturing is somewhat comparable to the welding process, most research is performed around alloys with acceptable weldability, such as IN718, Waspaloy, and Nimonic263 [115]. However, it is necessary to mention that the number of usable prevalent powders is not numerous and does not have a wide variety. Therefore, published papers regarding the additive manufacturing field of the NBSAs are mostly limited to a few specific and conventional grades [35].

Mainly three types of powders are used in the additive manufacturing processes of NBSAs:

- Powders with good weldability, like IN625, which avoid cracking because of solid solution strengthening and low content of precipitates [35, 116-120].
- Non-weldable powders that are susceptible to strain-age cracking because of gamma-prime (γ') precipitates.

In these alloys, the sum of the aluminum and titanium element content is typically more than 6.4%. The IN738 and CMSX-4 are among the examples of these alloys [53, 109, 121].

- Alloys with medium weldability are also part of NBSAs. In these cases, although the gamma-double prime secondary phase (γ'') precipitates in the matrix, this phase opposite of γ' does not face the specimen to considerably high strain age cracking. This precipitate-strengthening mechanism is used in the IN718 alloys. This balance between strength property and desired weldability has resulted in the general usage of IN718 in the additive manufacturing processes [1, 51, 122-131].

It is noteworthy that IN718 has proper weldability as well as structural and mechanical stability up to 650°C; therefore, this alloy is one of the most applicable additive manufacturing superalloys used in elevated-temperature applications, such as gas turbines and aviation engines. The IN718 is a superalloy made of nickel, iron, and chromium as the major elements in which the main strengthening precipitate is a semi-stable phase, γ'' , with a tetragonal body-centered cubic crystal structure [115]. The microstructural properties of the manufactured specimen and precipitates play a key role in the strengthening properties. Therefore, the characterization of the type, size, and dispersion of the precipitates has significant importance. The precipitate-strengthening properties in the IN718 are determined by the heat treatment cycle. Therefore, to reach the maximum mechanical properties, the heat treatment issues are bolded [115]. In this regard, different types of precipitates of the IN718 are listed in Table 3 [132].

Table 3. Existent phases in NBSAs [132]

	Phase	Crystal system	Primary Composition
Solid Solution Matrix	γ	Cubic	Ni, Cr, Fe-Based
	γ'	Cubic	$\text{Ni}_3(\text{Ti, Al, Nb})$
Intermetallic	γ''	Tetragonal	$\text{Ni}_3(\text{Nb, Ti})$
	δ	Orthorhombic	$\text{Ni}_3(\text{Nb, Ti})$
Topological	η	Hexagonal	$\text{Ni}_3(\text{Ti, Al})$
(Intermetallic)	Laves	Hexagonal	$(\text{Ni, Cr, Fe})_2(\text{Nb, Ti})$
	MC	Cubic	$(\text{Nb, Ti})(\text{C, N})$
Carbide	M_{23}C_6	Cubic	$(\text{Cr, Fe})_{23}\text{C}_6$

3. Comparison Between Additive Manufacturing and Conventional Methods in Manufacturing Steps and Resulting Microstructure

In previous sections, it was mentioned that one of the strengthening mechanisms of NBSAs is issued with secondary phase precipitates (γ' and γ''). In order to form and optimize this strengthening, the as-manufactured specimens must be heat-treated. Notably, because of their inherent variation from conventional methods, the AM-developed parts include secondary phases with smaller sizes. These differences between precipitate sizes are derived from a small melt pool, little time for secondary phases to join each other, and thereby less coring in the additive manufacturing processes [35, 51, 53, 62, 63, 106, 121, 123].

Regarding the past sections, it is clarified that all of the manufacturing steps in nickel-based additive manufacturing processes can influence the printed part properties. These steps include the following:

- Pre-manufacturing step and use of powder and chamber preheat [121]
- Manufacturing step and the process parameters [57, 109, 133]
- Scan strategy/pattern [62, 63]
- The post-process level and usage of heat treating [134]

Currently, accurate and obvious evaluation of the NBSAs properties in layer manufacturing/additive manufacturing is complex. Microstructural variations are derived from the process method, process parameters, and part geometry. All mentioned items simultaneously play a role in the mechanical properties, but the impact of each one and its share are not fully clear. After AM/forming/casting, NBSAs is mostly put under standard heat treatment. Nowadays, almost all studies regarding post-manufacturing heat treatment are based on the same information

received from the casting part. Therefore, due to the intrinsic disparities between the additive manufacturing structure and its counterparts, previously established standards may prove suboptimal in this context [25]. [35].

Furthermore, the mechanical properties, including the structure, display a non-equality/non-uniformity in the properties owing to different build directions. Currently, there are no standard samples for the mechanical tests of AM-developed parts. The standard sample should consider important properties of the layer manufacturing, such as surface roughness, post-processing, and build direction. Considering the impact of the build direction on the microstructure, in some reports, tests are carried out by sampling in both vertical and horizontal directions [35, 135].

3.1. Comparison Between Properties of Additive Manufacturing and Conventional Methods

In initial comparisons between additive manufacturing (DLD/LPBF) and conventional methods (wrought/casting), it was reported that heat-treated AM parts possess at least 80 % of the tensile strength of their wrought counterparts. Although LPBF outperforms DLD in as-deposited condition, DLD exhibits the lowest room-temperature tensile strength without heat treatment.

In most case studies, AM-produced samples demonstrate significantly greater elongation, exhibiting at least 25 % more elongation than wrought specimens [35, 106, 136]. The final part properties have been further enhanced by process-parameter optimization and machine upgrades—such as powder preheating. Recent studies have shown that, with appropriate heat treatment, creep properties of AM parts can exceed those of both wrought and cast components (Figure 5) [137].

Regardless of the influence of process parameters on pore formation, each AM process has inherent capability to achieve full density. Among conventional AM techniques, LPBF currently

delivers the highest part densities (Table 4). This superior densification is a key advantage of laser-based systems over electron-beam systems and underpins their enhanced mechanical performance [138]. Consequently, LBAM parts are regarded as more reliable for industrial applications, especially under extreme conditions such as those in gas turbine components.

Table 4. Densification capability of AM methods

Alloy/Element	Relative Density (%)	Process	Reference
AlSi10Mg	99.77±0.08	LPBF	[139]
Mg	95.28 to 96.13	LPBF	
Ta	99.6	LPBF	
Ti-6Al-4V	< 99	LPBF	
ABD-900 AM	99.9	LPBF	[26]
ABD-900 AM	98.4	EBPBF	
ABD-900 AM	99.92	EBPBF + HIP	
IN738LC	99.87 to 99.96	LPBF	[140]

3.2. Impact of Build Direction on the Mechanical Properties and its Comparison with the Casting Characteristics

The build direction directly influences the microstructure and properties of the part. In Figure 6, the two z and xy build directions are indicated [115, 141]. In the z-build direction, the specimen morphology is formed columnar parallel to the part axis. Nevertheless, in horizontal manufacturing of parts, the morphology similar to casting parts is manufactured in equiaxed form (xy-specimen in Figure 6).

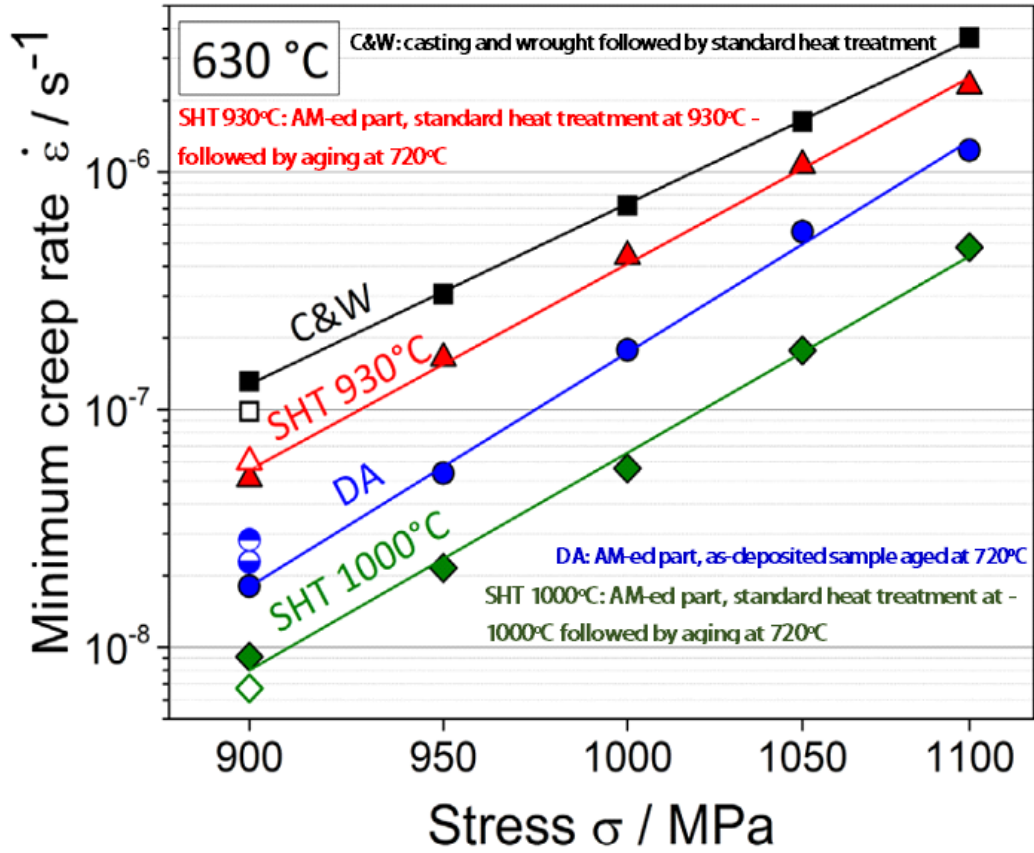


Fig. 5. Creep rate between 900 to 1100 MPa until 1% plastic deformation [137]

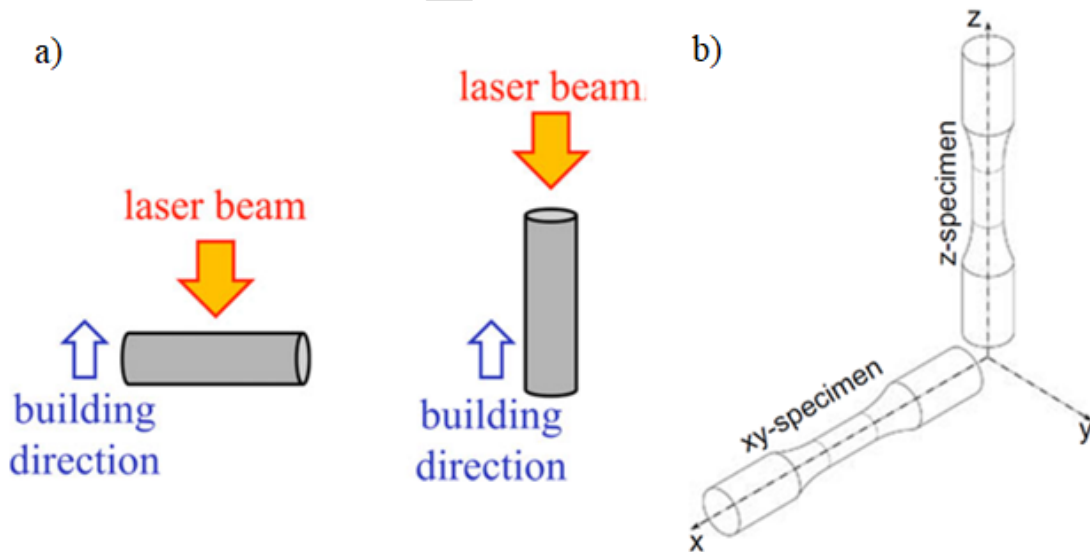


Fig. 6. (a) two various build directions in the LPBF build chamber [115], (b) schematic of the build direction concept [141]

Among the properties of NBSAs, creep is significant owing to the high-temperature applications of these alloys. Rickenbacher [141] et al. demonstrated that IN738 HIP samples manufactured in the vertical direction (z) have more creep strength compared to those manufactured in horizontal directions (xy). The creep strength of z specimens equals the minimum of the casting ones. Although the creep properties of the z specimen are better than xy, the other mechanical properties are less than xy. The comparison of tensile strength of the z specimen versus xy is according to Tables 5 and 6. This greater strength can be related to the impact of the hall-petch relation and grain boundary resistance against the dislocation movements in temperatures less than $0.5 T_m$.

Table 5. Tensile properties of the cast and LPBF samples at room temperature (IN738) at 23°C [141]

sample	Young's modulus (GPa)	$\sigma_{(0.2)}$ (MPa)	σ_{UTS} (MPa)	Elongation (%)
Casting reference	200	765	945	7.5
SLM-xy	233±9	933±8	1184±112	8.4±4.6
SLM-z	158±3	786±4	1162±35	11.2±1.9

Table 6. Tensile properties of the cast and LPBF samples at 850°C (IN738) [141]

sample	Young's modulus (GPa)	$\sigma_{(0.2)}$ (MPa)	σ_{UTS} (MPa)	Elongation (%)
Casting reference	144	530	710	10.0
SLM-xy	157±4	610±1	716±1	8.0±1.2
SLM-z	110±2	503±2	688±7	14.2±3.9

4. Scan Strategy Effect on the Mechanical Properties

The additive manufacturing scan strategy is an important item that highly impacts structural and mechanical properties. Many different scan patterns can be applied in part manufacturing. Scan patterns can include conventional linear and/or island patterns. In general, various forms of laser passes can be used on the specimen (Figure 7). Each of these forms induces a distinct transformation within the ultimate microstructure of the specimen. This variance in the resulting microstructure can be attributed to the fluctuation in the energy input applied to the powder and the final manufactured part. Overall, there are five common scan patterns, which can be seen in Figure 8 [35].

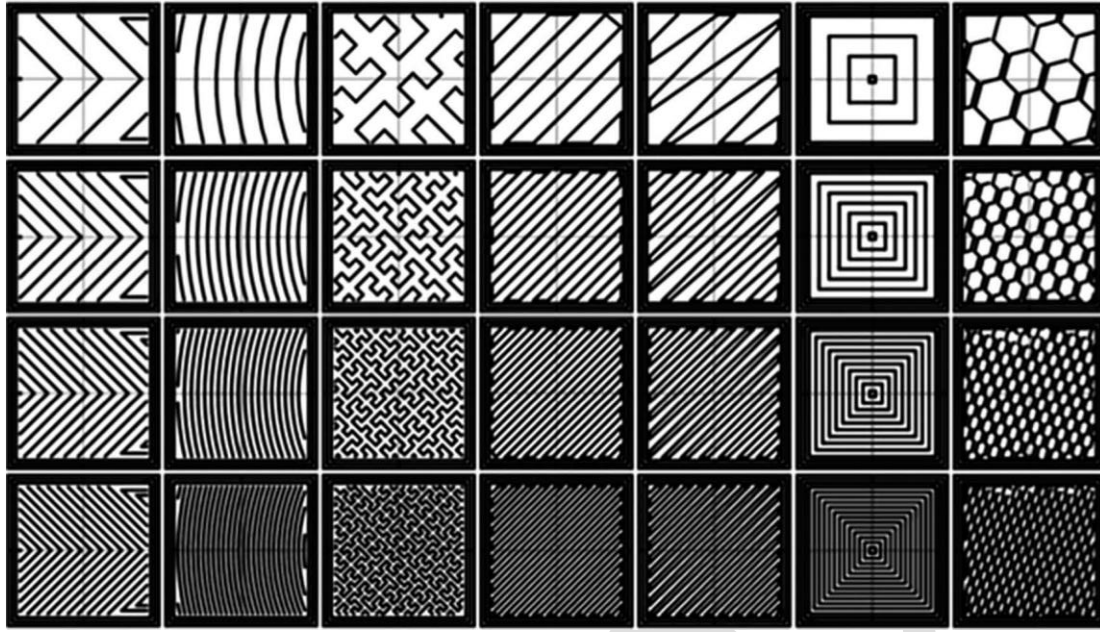


Fig. 7. Scan strategies influencing energy density and heat input, subsequently affecting microstructure and residual stress [35]

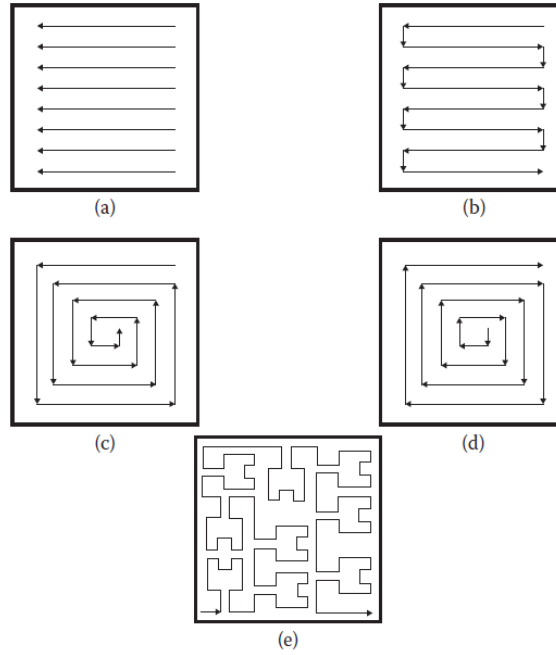


Fig. 8. Five conventional scan patterns [35]

According to scientific developments in the field of scan patterns, laser pass rotation in each layer is effective in improving the properties. After the deposition of each layer, the scan pattern is applied at a different angle to manufacture the next layer. Therefore, porosities in the part are reduced, and the sample density is near the theoretical density. The optimized angle in the literature is reported to be approximately 67° , between (30° and 90°). This strategy is also called the basket pattern [62, 63, 142, 143]; Figure 9 demonstrates the schematic image and the microstructure of a part with a basket pattern (more details are available in Section II.3).

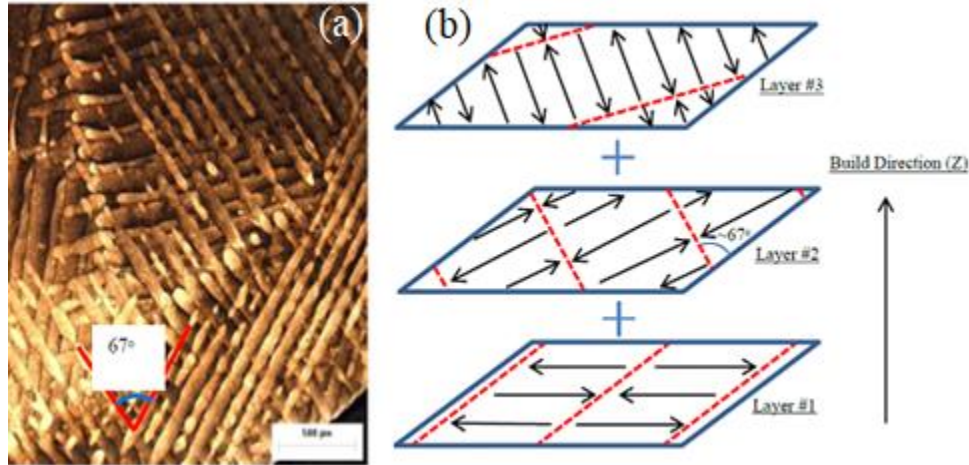


Fig. 9. a) Microstructure of the part with the interlayer rotation, b) A sample schematic of the rotation strategy [63]

4.1. Decrement of Residual Stress Using the Island Pattern

One of the significant problems in the additive manufacturing of parts is the residual stress in the sample and the deformation of the part. In order to avoid this problem, the island scan strategy is employed. Using conventional patterns, the energy diffuses focally to the sample, resulting in residual stress and distortion. To decrease the remaining stress, the energy is diffused dispersedly to the under-manufacturing specimen (Figure 10). The island strategy is used to satisfy this need. The manner may include various states. The totality of the island pattern is that the under-process layer is considered a raster, similar to a chess board. Each cell grid of the board is selected randomly and scanned by the laser beam to be manufactured. The random application of the energy to each cell causes the avoidance of focused energy inserted into one area of the part. The dispersed application of the energy inhibits part distortion and residual stress [144-148].

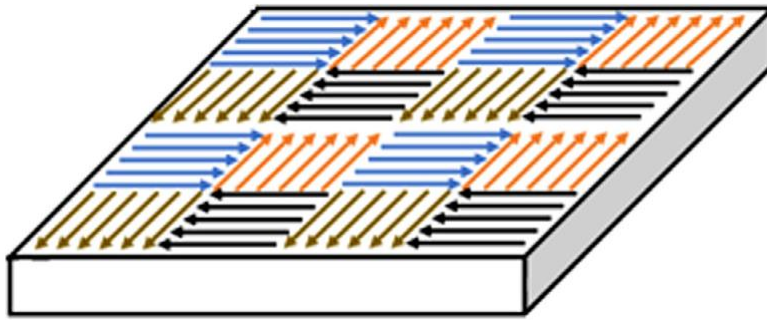


Fig. 10. Schematic of island scan strategy [148]

4.2. Hatch Spacing Distance

Hatch spacing is the distance between adjacent laser scan tracks. In general, hatch distances are chosen to ensure approximately 30% overlap between passes. For instance, if the melt pool diameter is $80\ \mu\text{m}$, a hatch spacing of around $60\ \mu\text{m}$ may be used to achieve this overlap [62, 149]. As presented in Equation 1, increasing the hatch spacing directly reduces the input energy. Improper selection of hatch spacing can lead to bonding defects, LOF, altered cooling rates, residual stresses, interlayer porosity [150, 151], surface roughness [36], and cracking [109]. In fact, most defects related to energy density can be influenced by hatch spacing. As noted by Saghaian et al. [152], this parameter can affect the microstructure, texture, and thermomechanical properties of alloys produced by LBAM (Figure 11). A complex relationship between hatch spacing and dwell time should also be considered when treating this as a variable parameter [2, 153].

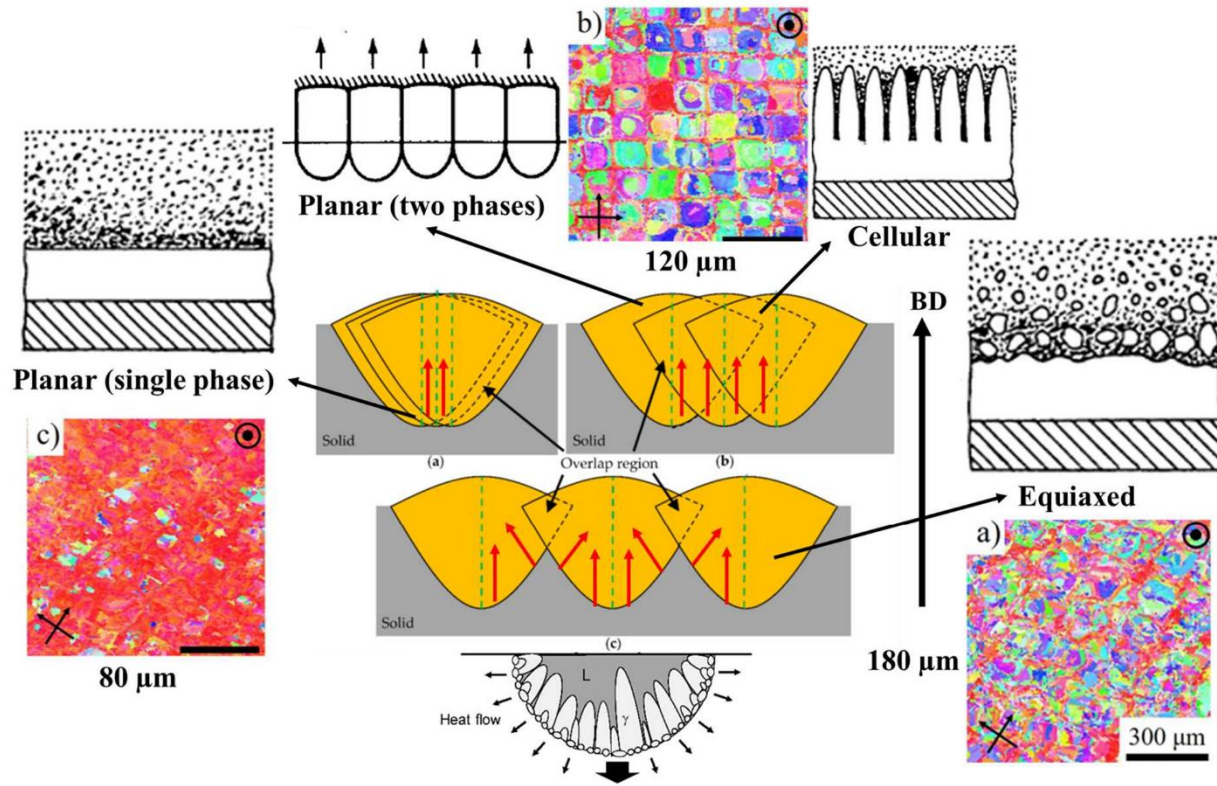


Fig. 11. Effect of hatch spacing on the microstructure in LPBF [152]

5. Defects (Pores and Cracks)

Parts produced via AM generally exhibit varying quality depending on the process parameters and/or feedstock used. The main defects observed in these parts are pores and cracks (Figure 12).

5.1. Cracks

The formation of cracks at the initial stage largely depends on the selection of raw materials. For this reason, weldable materials are predominantly used in AM processes. At later stages, process parameters significantly influence crack formation (Figure 13). The types of cracks reported in the literature for NBSAs are as follows:

- **Solidification Cracking**

When the volume fraction of the solid phase ranges between 0.7 and 0.9, the remaining liquid struggles to flow through the dendritic structure. Shrinkage of dendrites can lead to the formation of pores, which subsequently result in solidification cracks. This issue is particularly severe in non-weldable superalloys due to their pronounced segregation behavior. Also, solidification cracking is the most common type of cracking observed in solution-strengthened superalloys such as IN625 and Hastelloy X. These alloys contain elements like Hf, Nb, Mo, and C, which facilitate the formation of carbides and Laves phases. These phases exhibit low eutectic temperatures, which extend the mushy zone and increase the material's susceptibility to cracking.

- **Liquation Cracking**

Liquation cracking occurs when rapid heating prevents secondary phases from dissolving into the matrix, causing them to transition directly into a liquid phase. This liquid phase is unable to withstand the stresses induced by thermal contraction. Liquation cracking typically originates from eutectic phases, such as γ/γ' , and is most commonly observed in the heat-affected zone (HAZ). The presence of elements such as Si, Zr, and B can increase the susceptibility to liquation cracking in AM.

- **Strain-Age Cracking (SAC) and Ductility-Dip Cracking (DDC)**

These types of cracks occur in the solid state. Strain-age cracking (SAC) typically occurs in γ' strengthened superalloys with high Al and Ti content, which rely on precipitation strengthening. Ductility-dip cracking (DDC) has a more complex mechanism and is sometimes categorized as a form of liquation cracking or SAC.

To address the sensitivity of raw materials to crack defects, feedstock is typically selected from weldable NBSAs (Section III.2). However, in AM processes, due to rapid liquation and solidification, even weldable materials can become prone to cracking. Some researchers attribute cracks primarily to the energy input into the melt pool. A more comprehensive approach, however, involves examining the individual effects of each process parameter on defect formation. The range of process parameters influences the melt pool shape, liquation and solidification rates, and the heat-affected zone (HAZ). While these factors have been extensively studied, the results of current research are often inconsistent. For example, some studies report that increasing scan speed leads to higher crack density, while others present contradictory findings. Similar discrepancies are observed for laser power. One potential gap in the research is the limited consideration of element diffusion during AM processes. While only a few studies have investigated this aspect, some suggest that the presence of specific elements may significantly contribute to crack formation. Additionally, certain studies have noted the accumulation of elements, such as aluminum, around cracks, though these findings were incidental rather than the primary focus of investigation. Another cause of conflicting results across studies could be the limited parameter ranges considered and the lack of consistency in comparing results. For instance, the impact of increasing scan speed at low energy inputs may differ significantly from the same change at high energy levels. Table 7 presents the typical parameter ranges studied in the LPBF method, the most common AM technique for NBSAs.

5.2. Pores

It is common to observe pores in AM-produced parts after evaluation (Figure 13a). The origins of these pores can be categorized into two main types. The first type of pores results from LOF. LOF defects occur when the laser source fails to adequately melt the substrate or raw material. The

second type originates from entrapped gases within the sample. These gases can form under various conditions. For instance, improper production methods of AM powder may introduce gases into the raw material, which are subsequently transferred to the part during the AM process. Additionally, some gases are produced due to the evaporation of volatile elements in the melt pool. This type of pore can be minimized by optimizing the process parameters. High energy input to the melt pool, achieved by decreasing the scan speed or increasing laser power, alters the melt pool shape. Specifically, increasing the energy input transforms the melt pool shape from a teardrop to an elliptical form. This change increases the width-to-depth ratio of the melt pool, facilitating the escape of trapped pores.

As mentioned before, some studies associate defect formation with the energy input to the melt pool, while others focus on the individual effects of process parameters. The values of process parameters can vary widely, as shown in Table 7. Most investigations have explored the influence of parameters in the high scan speed range. However, at low scan speeds, even small changes in speed can lead to significant variations in energy input, as indicated by Equation 1. This highlights a research gap in the low scan speed range that warrants further investigation.

$$E = \frac{P}{v \times t \times h} \quad (1)$$

Where P is the laser power (W), v is the scan speed (mm/s), t is the layer thickness (mm), and h is the hatch spacing (mm).

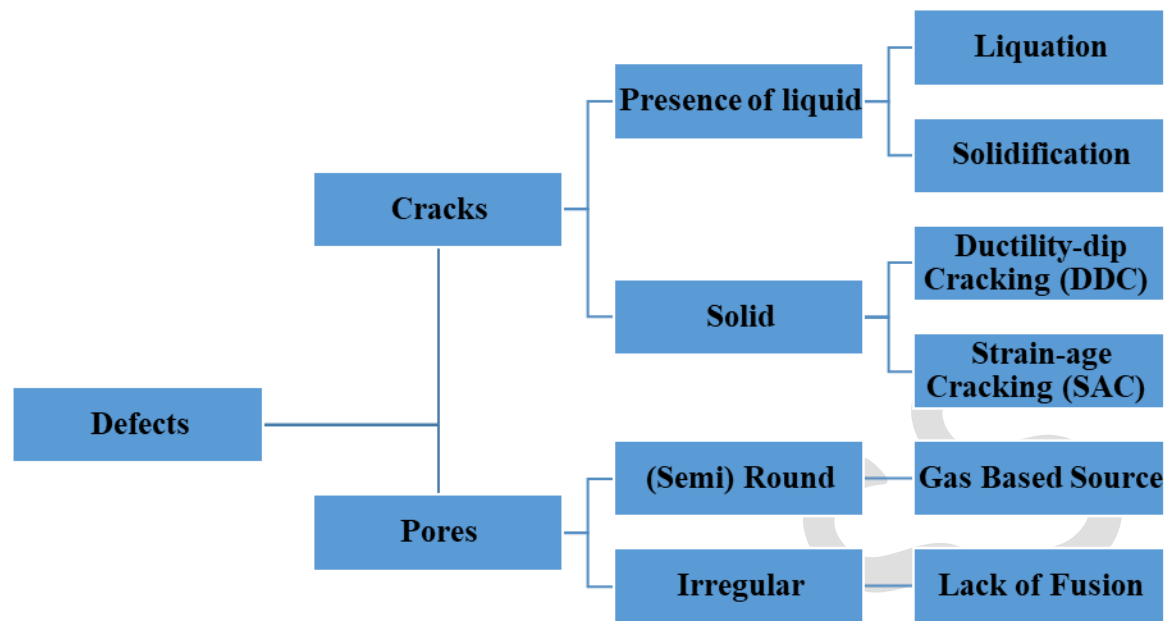


Figure 12. Common defects in LBAM of NBSAs [36, 109, 139]

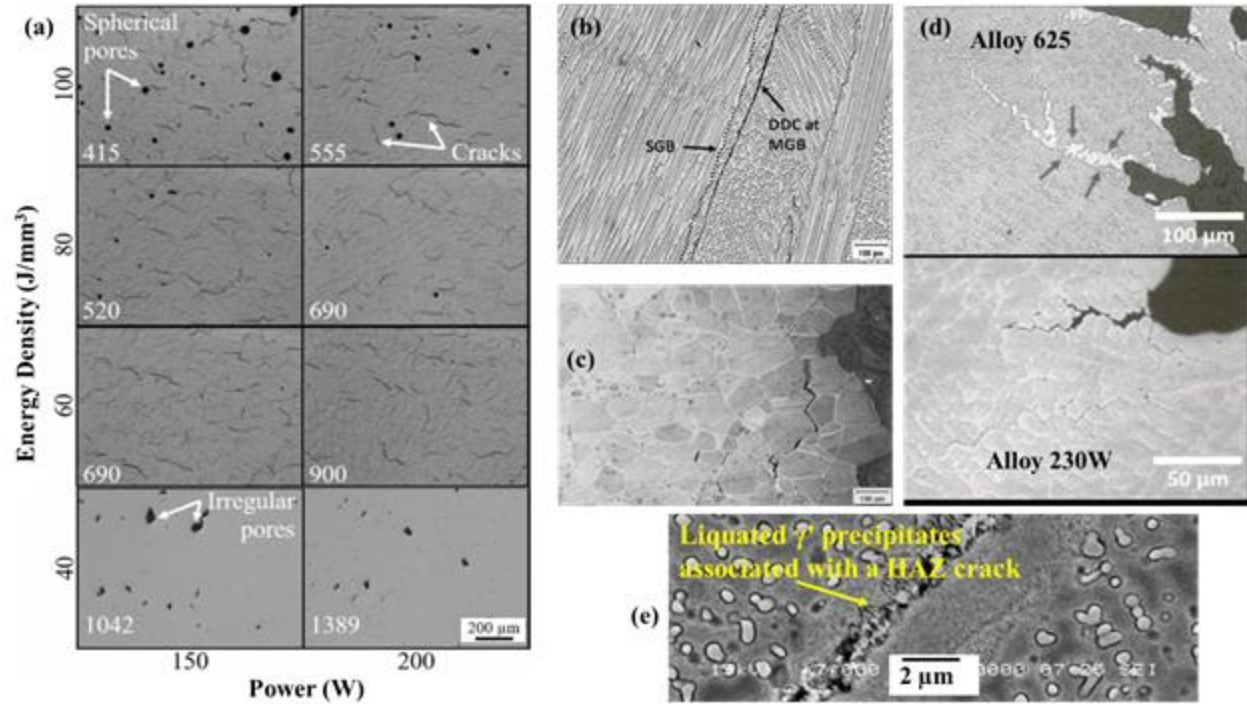


Figure 13. (a) Various pores, including spherical and irregular types, and cracks observed under different process parameters in LPBF of IN625; white numbers indicate scan speeds [154], (b) DDC in Ni-based weld metal along a migrated grain boundary (MGB); the dotted line represents the solidification grain boundary (SGB) [155], (c) SAC: intergranular strain-assisted cracking (SAC) in the simulated HAZ of Waspalloy [155], (d) Solidification cracking; the white area indicated by arrows is a Nb-rich eutectic [156], (e) Liquation cracking in the HAZ of Ni-based superalloy welds [157]

Table 7. Common range of LPBF process parameters

Scan Speed Range	Power Range	Layer Thickness	Weldability (Superalloy)	Descriptions	Reference
725 to 875 mm/s	169 to 195 w	20 μm	625	Hatch= 90 to 110 μm	[۱۵۹, ۱۵۸]
320 to 1250 mm/s	156 to 195 w	20 to 40 μm	IN625	Hatch= 80 to 100 μm	[۱۶۰]
1000 to 1300 mm/s	100 to 170 w	20 μm	non- weldable MAD542 and ME3	Hatch= 50 to 70 μm	[۱۶۱]
1000 to 1900 mm/s	170 to 195 w	20 μm	Rene 80 non- weldable	Hatch= 30 to 80 μm	[۱۶۲]
2800 to 3200 mm/s	170 to 220 w	20 μm	247 LC non- weldable	Hatch= 20 to 40 μm	[۱۶۳]
200 to 2200 mm/s	125 to 350 w	30 μm	IN718, weldable	Hatch= 60 and 120 μm	[۱۶۴]
800 mm/s	195 w	20 μm	IN625, weldable	Hatch= 100 μm , changing in Scan strategy	[۱۶۵]
500 to 1000 mm/s	170w	30 μm	IN718	30% overlap between passes,	[۶۲]

				Hatch= 56 μm , laser spot= 80 μm	
800 to 1400 mm/s	200 w	30 μm	K418, medium weldability	Hatch= 70 μm Al+Ti=4.3%	[۱۶۶]
400-2000 mm/s	100-200 w	20 μm	CM247 LC non- weldable, directional solidified	Laser spot: 150 μm	[۱۰۹]
500-1500 mm/s	150-350w	30-62 μm	IN718 weldable	(Optimized) P=245-255w V= 850-1000 mm/s Hatch: 100-110 μm Layer thickness: 43- 48 μm Beam diameter: 100 μm	[۱۲]
150 to 250 mm/s	400 to 600 w	1.4 mm	CMSX-4 non- weldable	Selective laser epitaxy (SLE), Layer thickness and hatch: 1 to 2 mm	[۱۶۷]

6. A Commentary on Additive Manufacturing of Gamma-Prime Inducing NBSAs

As mentioned earlier, the superalloys with a sum of aluminum and titanium greater than 6.4% are sorted as non-weldable alloys. Two conventional grades of this non-weldable group are IN738 and CMSX-4. Defectless joining in these alloys without using preheat is so difficult practically. In these alloys, strain-age cracks are created in the specimen due to the formation of the gamma-prime phase. In order to solve the problem, preheat facilities have been designed for some new additive manufacturing machines. For the proper joining of superalloys like IN738, the preheat

temperature is usually set between 650°C to 800°C; applying this temperature makes the process hard in structure. Despite complex manufacturing, some advantages include small gamma primes and more homogenous distribution in the AM-developed parts.

Conversely, the manufacturability of components with intricate internal cooling channels, such as new turbine blades, has catalyzed research efforts toward the exploration of additive manufacturing techniques for these particular alloys. Moreover, in single crystal grades, including CMSX-4, AM-developed parts are prone to form columnar structure, and it is possible to customize the structure to a large extent. Therefore, much research has been carried out regarding the effect of the process parameters on the type of solidifying structure and columnarization of the grains [111, 168-179].

7. Microscopy

Two important items in the non-weldable superalloys are the size and distribution of the gamma prime particles. As mentioned, the present gamma primes in the AM-developed parts are smaller than those in the cast parts. In order to receive an acceptable image of the existing gamma primes in the parts, it is necessary to use a proper etchant solution to prepare them.

- Marble's solution is proper because it preferentially attacks the gamma prime phase and leaves the residual gamma-matrix unaffected. The composition of Marble's solution is as follows [180]:

50 ml HCl, 50 ml H₂O, and 10 mg CuSO₄

- Another conventional reagent has the following composition [181]:

10 ml HNO₃, 50 ml HCl, and 60 ml glycerol

- For a proper electrical etch, the following composition may be used. It is noteworthy that the process is carried out in 6 V for about 5 s [182-186].



8. Applicable Mechanical Tests

In general, numerous mechanical tests may be used to evaluate the mechanical properties of one specimen made of NBSAs. Different types of tests are employed to determine the working conditions of the sample. For instance, NBSAs often has elevated/high-temperature applications; therefore, the creep test is highly important. Fatigue [187], room and high-temperature tensile strength [147, 188-194], punch and tensile creep [195-203], relaxation, hardness, and micro-hardness [147, 204, 205] tests may be specimen evaluation metrics. Some tests are used to predict the material properties in another test. For example, if the creep test is not practically possible, the relaxation test can be employed to have a total assumption of the material properties [115].

9. Improvement of AM-Developed Part Properties by HIP Treatment

If the LPBF- and DLD-developed parts are subjected to heat treatment or HIP, the final properties will be comparable to the parts produced via conventional methods. Primarily for AM-developed parts, the same conventional heat treatment is applied to casting parts. However, it is evident that the traditional heat treatment process is an objective initiation point and needs to be improved and adapted for AM-developed parts [35, 206]. Therefore, much research is needed in this regard.

By employing HIP, nearly all cracks are removed from susceptible alloys, such as IN738, and the porosities become small. By this method, only the internal cracks (the cracks connected to the surface remain) are eliminated. Machining can be employed to eliminate near-surface cracks with

interconnections; however, this approach may be infeasible in instances where the sample's geometry precludes such intervention [109, 141].

10. Advantages of Segregation Reduction and Homogeneity Enhancement in AM

Another advantage of AM-developed parts is their improved chemical homogeneity, which is attributed to the small melt pool size in AM processes. Due to rapid solidification and limited melt volume, alloying elements have insufficient time to segregate during solidification. In contrast, cast specimens typically exhibit greater elemental segregation. In casting, alloying elements are pushed toward the remaining melt as solidification progresses, resulting in significant composition gradients between the initial and final solidified regions [34, 141, 207]. Rickenbacher et al. [141] illustrated this behavior by plotting the composition variation range in cast specimens and demonstrated that it is significantly higher than in AM-developed counterparts.

11. New Materials

Nowadays, due to the previously mentioned challenges in processing γ' -inducing NBSAs, studies have been conducted on modified materials. NBSAs were conventionally produced by casting; therefore, their chemical compositions were tailored to achieve the required properties after casting. In recent years, the same cast alloys have been used in AM processes. Some materials, such as IN738, retain their strength and performance at high temperatures and in extreme environments due to the presence of the γ' phase [208]. However, as discussed earlier in Section III.2, their inherent properties lead to poor weldability and, consequently, poor AM processability. Recent studies have shown that crack-free LBAM of these traditionally non-weldable alloys is possible, provided that process parameters are carefully selected [209]. These parameters often require re-optimization for each new experimental condition, such as variations in geometry,

powder composition, or particle size [210]. However, in industrial applications with complex geometries, achieving crack-free production remains a significant challenge. To address these issues, efforts have been made to reduce the content of γ' -forming elements such as Al and Ti. In addition, some studies have aimed to modify the chemical composition to narrow the solidification range, thereby minimizing the risk of solidification cracking. ABD-900AM is one such newly designed superalloy. After proper heat treatment, it forms approximately 35% γ' by volume. In these alloys, the reduced γ' strengthening is compensated by the addition of solid-solution strengthening elements such as W and Mo, which strengthen the γ phase. The resulting mechanical properties at high temperatures are comparable to those of IN738 and IN739, which are commonly used in turbine blades and hot-section nozzles of gas turbines [26, 211-216].

IV. Conclusion

The review begins by addressing the progress and development of LBAM (DLD and LPBF), providing a foundation for understanding the evolving capabilities and limitations of these methods in industry. By exploring the development trajectory of LBAM, we gain deeper insight into how LPBF and DLD can be optimized and applied across various applications. The second half of the review focuses on a case study of nickel alloys, emphasizing how the knowledge of LBAM's evolution helps to better understand the potential and challenges of these techniques in the context of specific materials.

The findings of this review indicate that, LPBF and DLD are transforming the manufacturing landscape for NBSAs, offering significant advantages for the fabrication and repair of complex components. Traditional methods like casting and wrought processing are constrained by geometric limitations, long lead times, and difficulties in defect control. In contrast, LPBF and DLD can produce net-shape parts with intricate geometries, reducing material waste and offering localized heat input for improved microstructures. This review has highlighted key aspects of the processes, including powder characteristics, laser-material interaction, thermal cycling, and microstructural evolution, with a particular focus on how processing parameters influence final part quality.

The processability of various NBSAs in AM has been a central theme, with weldable alloys like IN625 being more amenable to LPBF and DLD, while more challenging alloys such as IN718 and non-weldable NBSAs like IN738 and CMSX-4 require tailored strategies to overcome processing difficulties. Moreover, the review underscores the need for developing AM-specific post-processing treatments, as traditional methods do not effectively address the unique microstructures of AM-produced components.

Emerging trends such as in-situ monitoring, machine learning-based optimization, and the development of crack-resistant alloys are essential for advancing AM's reliability and repeatability. As research progresses, AM will continue to enable the production and repair of advanced NBSA components with customized performance, offering promising implications for sectors such as aerospace and power generation. The continued exploration of processing strategies, alloy design, and microstructure-property relationships will be crucial to fully realizing the potential of LPBF and DLD in industrial applications.

❖ Conflict of Interest

All co-authors have seen and agree with the contents of the manuscript and there is no financial interest to report.

References

1. Wang, X., Gong, X. and Chou, K., "Review on powder-bed laser additive manufacturing of Inconel 718 parts," *Proc. Inst. Mech. Eng. B J. Eng. Manuf.*, 2017, 231(11), 1890–1903. <https://doi.org/10.1177/0954405415619883>
2. Thompson, S. M., Bian, L., Shamsaei, N. and Yadollahi, A., "An overview of Direct Laser Deposition for additive manufacturing; Part I: Transport phenomena, modeling and diagnostics," *Addit. Manuf.*, 2015, 8, 36–62. <https://doi.org/10.1016/j.addma.2015.07.001>
3. Nayak, S., Mishra, S., Jinoop, A., Paul, C. and Bindra, K., "Experimental studies on laser additive manufacturing of Inconel-625 structures using powder bed fusion at 100 μm layer thickness," *J. Mater. Eng. Perform.*, 2020, 29, 7636–7647. <https://doi.org/10.1007/s11665-020-05215-9>
4. Luu, D. N., Zhou, W. and Nai, S. M. L., "Mitigation of liquation cracking in selective laser melted Inconel 718 through optimization of layer thickness and laser energy density," *J. Mater. Process. Technol.*, 2022, 299, 117374. <https://doi.org/10.1016/j.jmatprotec.2021.117374>
5. Nguyen, Q., Luu, D., Nai, S., Zhu, Z., Chen, Z. and Wei, J., "The role of powder layer thickness on the quality of SLM printed parts," *Arch. Civ. Mech. Eng.*, 2018, 18(3), 948–955. <https://doi.org/10.1016/j.acme.2018.01.015>
6. Paradise, P., Pannala, S., Babu, S., Plotkowski, A., Kirka, M., Dehoff, R. and Paquit, V., "Improving Productivity in the Laser Powder Bed Fusion of Inconel 718 by Increasing Layer Thickness: Effects on Mechanical Behavior," *J. Mater. Eng. Perform.*, 2022, 31(8), 6205–6220. <https://doi.org/10.1007/s11665-022-06961-8>
7. Knapp, G. L., Raghavan, N., Plotkowski, A. and Debroy, T., "Experiments and simulations on solidification microstructure for Inconel 718 in powder bed fusion electron beam additive manufacturing," *Addit. Manuf.*, 2019, 25, 511–521. <https://doi.org/10.1016/j.addma.2018.12.001>
8. Nandwana, P., Kirka, M., Okello, A. and Dehoff, R., "Electron beam melting of Inconel 718: effects of processing and post-processing," *Mater. Sci. Technol.*, 2018, 34(5), 612–619. <https://doi.org/10.1080/02670836.2018.1424379>
9. Sames, W. J., Unocic, K. A., Helmreich, D., Dehoff, R. R., Babu, S. S. and Love, L. J., "Feasibility of in situ controlled heat treatment (ISHT) of Inconel 718 during electron beam melting additive manufacturing," *Addit. Manuf.*, 2017, 13, 156–165. <https://doi.org/10.1016/j.addma.2016.09.001>
10. Helmer, H., Bauereiß, A., Singer, R. and Körner, C., "Grain structure evolution in Inconel 718 during selective electron beam melting," *Mater. Sci. Eng. A*, 2016, 668, 180–187. <https://doi.org/10.1016/j.msea.2016.05.046>
11. Gu, D., Shi, X., Poprawe, R., Zhou, W. and Meiners, W., "Densification behavior, microstructure evolution, and wear performance of selective laser melting processed commercially pure titanium," *Acta Mater.*, 2012, 60(9), 3849–3860. <https://doi.org/10.1016/j.actamat.2012.04.006>
12. Lu, C. and Shi, J., "Simultaneous consideration of relative density, energy consumption, and build time for selective laser melting of Inconel 718: A multi-objective optimization study on process parameter selection," *J. Clean. Prod.*, 2022, 369, 133284. <https://doi.org/10.1016/j.jclepro.2022.133284>

13. Riazi, A. H., Boutorabi, S. M. A., Aboutalebi, M. and Shabani, M. O., “*Design of gating system for propeller casting through melt flow simulation*,” Int. J. Comput. Mater. Sci. Surf. Eng., 2022, 11(1), 47–71. <https://doi.org/10.1504/IJCMSSE.2022.125744>
14. Blakey-Milner, B., Mognol, P., Laverne, F., Lachaud, F., Gaillard, P. and Buffière, J.-Y., “*Metal additive manufacturing in aerospace: A review*,” Mater. Des., 2021, 209, 110008. <https://doi.org/10.1016/j.matdes.2021.110008>
15. Liu, Z., Li, C., Fang, X. and Guo, Y., “*Energy consumption in additive manufacturing of metal parts*,” Procedia Manuf., 2018, 26, 834–845. <https://doi.org/10.1016/j.promfg.2018.07.104>
16. Popovich, A. A., Sufiarov, V. S., Borisov, E. V., Polozov, I. A. and Masaylo, D. V., “*Design and Manufacturing of Tailored Microstructure with Selective Laser Melting*,” Mater. Phys. Mech., 2018, 38(1), 1–10. http://dx.doi.org/10.18720/MPM.3812018_1
17. Aboutaleb, A. M., Bian, L., Elwany, A., Shamsaei, N., Thompson, S. M. and Tapia, G., “*Accelerated process optimization for laser-based additive manufacturing by leveraging similar prior studies*,” IISE Trans., 2017, 49(1), 31–44. <https://doi.org/10.1080/0740817X.2016.1189629>
18. Khoda B, Benny T, Rao P K, Sealy M P and Zhou C, Applications of laser-based additive manufacturing. Laser-Based Additive Manufacturing of Metal Parts, ed. Bian L, Shamsaei N and Usher J, CRC Press, Boca Raton, USA, 2017, 240–288. <https://doi.org/10.1201/9781315151441>
19. Moghaddam N S, Jahadakbar A, Amerinatanzi A and Elahinia M, Recent advances in laser-based additive manufacturing. Laser-Based Additive Manufacturing of Metal Parts, ed. Bian L, Shamsaei N and Usher J, CRC Press, Boca Raton, USA, 2017, 2–23. <https://doi.org/10.1201/9781315151441>
20. Rashid, M., Sabu, S., Kunjachan, A., Agilan, M., Anjilivelil, T. and Joseph, J., “*Advances in wire-arc additive manufacturing of nickel-based superalloys: Heat sources, DfAM principles, material evaluation, process parameters, defect management, corrosion evaluation and post-processing techniques*,” Int. J. Lightw. Mater. Manuf., 2024. <https://doi.org/10.1016/j.ijlmm.2024.05.009>
21. Wu, B., Zhang, Y., Liu, J., Wang, Q., Zhao, L. and Li, S., “*Selective crack propagation in steel-nickel component printed by wire arc directed energy deposition*,” Mater. Des., 2024, 237, 112541. <https://doi.org/10.1016/j.matdes.2023.112541>
22. Henderson, M., Arrell, D., Larsson, R., Heobel, M. and Marchant, G., “*Nickel based superalloy welding practices for industrial gas turbine applications*,” Sci. Technol. Weld. Join., 2004, 9(1), 13–21. <https://doi.org/10.1179/136217104225017099>
23. Jena, A., Atabay, S. E. and Brochu, M., “*Microstructure and mechanical properties of crack-free Inconel 738 fabricated by laser powder bed fusion*,” Mater. Sci. Eng. A, 2022, 850, 143524. <https://doi.org/10.1016/j.msea.2022.143524>
24. Giuliani, F., Paulitsch, N., Cozzi, D., Görtler, M. and Andracher, L., “*An assessment on the benefits of additive manufacturing regarding new swirler geometries for gas turbine burners*,” in Turbo Expo: Power for Land, Sea, and Air, 2018, 51050, V04AT04A008. <https://doi.org/10.1115/GT2018-75165>
25. Cecconi, M. and Giovannetti, I., “*Development of Additive Manufacturing Gas Turbine Hot Gas Path Vanes at Baker Hughes*,” in Turbo Expo: Power for Land, Sea, and Air, 2023, 87066, V11BT23A005. <https://doi.org/10.1115/GT2023-103043>

26. Bridges, A. and Shingledecker, J., “*Creep Deformation and Damage Mechanisms in an Advanced High-Temperature Additively Manufactured Nickel-Base Superalloy*,” JOM, 2025, pp. 1–22.
<https://doi.org/10.1007/s11837-025-07326-x>
27. Avdoyic, P., Galiasevic, M., Navotsky, V. and Graichen, A., “ICDBY3D Intelligent Component Development for Gas Turbine by Using 3D Printing at Siemens Energy AB Sweden,” Proceedings of the International Conference New Technologies, Development and Applications, Springer, 2021, 286–300.
https://doi.org/10.1007/978-3-030-75275-0_33
28. Kover, A., “*Transformation in 3D: How a walnut-sized part changed the way GE aviation builds jet engines*,” last modified November 19, 2018. <https://amtil.com.au/transformation-in-3d-how-a-walnut-sized-part-changed-how-ge-aviation-builds-jet-engines/>
29. Bose, S. and Bandyopadhyay, A., “*Additive manufacturing: the future of manufacturing in a flat world*,” in Additive Manufacturing, Second Edition, CRC Press, 2019, 451–461.
<https://doi.org/10.1201/9780429466236>
30. Hu, D. and Kovacevic, R., “*Sensing, modeling and control for laser-based additive manufacturing*,” Int. J. Mach. Tools Manuf., 2003, 43(1), 51–60. [https://doi.org/10.1016/S0890-6955\(02\)00163-3](https://doi.org/10.1016/S0890-6955(02)00163-3)
31. Calta, N. P., Jung, S., Duchin, J., Babu, S. S., & Brown, D. W., “*Pressure dependence of the laser-metal interaction under laser powder bed fusion conditions probed by in situ X-ray imaging*,” Addit. Manuf., 2020, 32, 101084. <https://doi.org/10.1016/j.addma.2020.101084>
32. Yan, Z., Yu, J., Wang, F., Xu, X., & Liu, Y., “*Review on thermal analysis in laser-based additive manufacturing*,” Opt. Laser Technol., 2018, 106, 427–441.
<https://doi.org/10.1016/j.optlastec.2018.04.034>
33. Singh, S., Sharma, V., & Sachdeva, A., “*Progress in selective laser sintering using metallic powders: a review*,” Mater. Sci. Technol., 2016, 32(8), 760–772.
<https://doi.org/10.1179/1743284715Y.00000000136>
34. Körner, C., Brandl, E., & Heinel, P., “*Microstructure and mechanical properties of CMSX-4 single crystals prepared by additive manufacturing*,” Metall. Mater. Trans. A, 2018, 49, 3781–3792.
<https://doi.org/10.1007/s11661-018-4762-5>
35. Bian L, Shamsaei N and Usher J M, Laser-Based Additive Manufacturing of Metal Parts: Modeling, Optimization, and Control of Mechanical Properties. CRC Press, Boca Raton, USA, 2017, 65.
<https://doi.org/10.1201/9781315151441>
36. Mostafaei, A., Shamsaei, N., Bian, L., Yadollahi, A., & Elwany, A., “*Additive Manufacturing of Nickel-based superalloys: a state-of-the-art review on process-structure-defect-property relationship*,” Prog. Mater. Sci., 2023, 101108. <https://doi.org/10.1016/j.pmatsci.2023.101108>
37. Sanchez, S., Mukherjee, T., & Shamsaei, N., “*Powder Bed Fusion of nickel-based superalloys: A review*,” Int. J. Mach. Tools Manuf., 2021, 165, 103729.
<https://doi.org/10.1016/j.ijmachtools.2021.103729>
38. Kuntoğlu, M., Demirci, E., & Karadeniz, H., “*A review on microstructure, mechanical behavior and post processing of additively manufactured Ni-based superalloys*,” Rapid Prototyp. J., 2024, 30(9), 1890–1910. <https://doi.org/10.1108/RPJ-10-2023-0380>

39. Zhang, Y., Yan, C., Zhu, H., & Chen, X., “Additive manufacturing of metallic materials: a review,” *J. Mater. Eng. Perform.*, 2018, 27(1), 1–13. <https://doi.org/10.1007/s11665-017-2747-y>
40. Khimich, M. A., Ibragimov, E. A., Saprykina, N. A., Sharkeev, Y. P., & Saprykin, A. A., “Co-Cr-Mo alloy produced via powder bed laser fusion,” *AIP Conf. Proc.*, 2020, 2310(1), 020144. <https://doi.org/10.1063/5.0034111>
41. Liu, Y., Yang, Y., & Wang, D., “A study on the residual stress during selective laser melting (SLM) of metallic powder,” *Int. J. Adv. Manuf. Technol.*, 2016, 87(1), 647–656. <https://doi.org/10.1007/s00170-016-8466-y>
42. Kumar, M. S., Jeyaprakash, N., & Yang, C.-H., “Role of layer thickness on the damage mechanism in the LPBFed copper alloy,” *Arch. Civ. Mech. Eng.*, 2024, 24(3), 1–22. <https://doi.org/10.1007/s43452-024-00983-w>
43. Liu, J., Shi, Y., Lu, Z., & Huang, S., “Manufacturing near dense metal parts via indirect selective laser sintering combined with isostatic pressing,” *Appl. Phys. A*, 2007, 89(3), 743–748. <https://doi.org/10.1007/s00339-007-4159-6>
44. Dewidar, M. M. A., “Direct and indirect laser sintering of metals,” PhD Thesis, University of Leeds, 2002.
45. Maeda, K., & Childs, T., “Laser sintering (SLS) of hard metal powders for abrasion resistant coatings,” *J. Mater. Process. Technol.*, 2004, 149(1-3), 609–615. <https://doi.org/10.1016/j.jmatprotec.2004.02.024>
46. Yakout, M., Elbestawi, M., & Veldhuis, S. C., “A review of metal additive manufacturing technologies,” *Solid State Phenom.*, 2018, 278, 1–14. <https://doi.org/10.4028/www.scientific.net/SSP.278.1>
47. Yap, C. Y., Chua, C. K., Dong, Z. L., Liu, Z. H., Zhang, D. Q., & Loh, L. E., “Review of selective laser melting: Materials and applications,” *Appl. Phys. Rev.*, 2015, 2(4), 041101. <https://doi.org/10.1063/1.4935926>
48. Byun, Y., Kim, D. K., Lee, J. H., & Kim, Y. W., “Effects of Cr and Fe addition on microstructure and tensile properties of Ti–6Al–4V prepared by direct energy deposition,” *Metals Mater. Int.*, 2018, 24(6), 1213–1220. <https://doi.org/10.1007/s12540-018-0148-x>
49. Zhang, C., Huang, Y., & Chen, C., “Additive manufacturing of functionally graded materials: A review,” *Mater. Sci. Eng. A*, 2019, 764, 138209. <https://doi.org/10.1016/j.msea.2019.138209>
50. Ghanavati, R., & Naffakh-Moosavy, H., “Additive manufacturing of functionally graded metallic materials: A review of experimental and numerical studies,” *J. Mater. Res. Technol.*, 2021, 13, 1628–1664. <https://doi.org/10.1016/j.jmrt.2021.05.022>
51. Hosseini, E., & Popovich, V., “A review of mechanical properties of additively manufactured Inconel 718,” *Addit. Manuf.*, 2019, 30, 100877. <https://doi.org/10.1016/j.addma.2019.100877>
52. Yilmaz, O., & Ugla, A. A., “Shaped metal deposition technique in additive manufacturing: A review,” *Proc. Inst. Mech. Eng. Part B J. Eng. Manuf.*, 2016, 230(10), 1781–1798. <https://doi.org/10.1177/0954405416640181>

53. Ramakrishnan, A., & Dinda, G., "Direct laser metal deposition of Inconel 738," *Mater. Sci. Eng. A*, 2019, 740, 1–13. <https://doi.org/10.1016/j.msea.2018.10.020>
54. Shamsaei, N., Yadollahi, A., Bian, L., & Thompson, S. M., "An overview of Direct Laser Deposition for additive manufacturing; Part II: Mechanical behavior, process parameter optimization and control," *Addit. Manuf.*, 2015, 8, 12–35. <https://doi.org/10.1016/j.addma.2015.07.001>
55. Prashanth, K. G., Scudino, S., Maity, T., Das, J., & Eckert, J., "Is the energy density a reliable parameter for materials synthesis by selective laser melting?," *Mater. Res. Lett.*, 2017, 5(6), 386–390. <https://doi.org/10.1080/21663831.2017.1299808>
56. Yusuf, S. M., & Gao, N., "Influence of energy density on metallurgy and properties in metal additive manufacturing," *Mater. Sci. Technol.*, 2017, 33(11), 1269–1289. <https://doi.org/10.1080/02670836.2017.1289444>
57. Pleass, C., & Jothi, S., "Influence of powder characteristics and additive manufacturing process parameters on the microstructure and mechanical behaviour of Inconel 625 fabricated by Selective Laser Melting," *Addit. Manuf.*, 2018, 24, 419–431. <https://doi.org/10.1016/j.addma.2018.09.023>
58. Mahamood, R., & Akinlabi, E., "Effect of Powder Flow Rate on Surface Finish in Laser Additive Manufacturing Process," in *IOP Conf. Ser. Mater. Sci. Eng.*, 2018, 391(1), 012005. <https://doi.org/10.1088/1757-899X/391/1/012005>
59. Bhardwaj, T., Shukla, M., Paul, C., & Bindra, K., "Direct energy deposition-laser additive manufacturing of titanium-molybdenum alloy: Parametric studies, microstructure and mechanical properties," *J. Alloys Compd.*, 2019, 787, 1238–1248. <https://doi.org/10.1016/j.jallcom.2019.02.121>
60. Walker, T., Bennett, C., Lee, T., & Clare, A., "A novel numerical method to predict the transient track geometry and thermomechanical effects through in-situ modification of the process parameters in Direct Energy Deposition," *Finite Elem. Anal. Des.*, 2020, 169, 103347. <https://doi.org/10.1016/j.finel.2019.103347>
61. Masaylo, D., Igoshin, S., Popovich, A., & Popovich, V., "Effect of process parameters on defects in large scale components manufactured by direct laser deposition," *Mater. Today Proc.*, 2020, 30, 665–671. <https://doi.org/10.1016/j.matpr.2020.01.519>
62. Amirjan, M., & Sakiani, H., "Effect of scanning strategy and speed on the microstructure and mechanical properties of selective laser melted IN718 nickel-based superalloy," *Int. J. Adv. Manuf. Technol.*, 2019, 103(5), 1769–1780. <https://doi.org/10.1007/s00170-019-03545-0>
63. Anam, M. A., Dilip, J., Pal, D., & Stucker, B., "Effect of scan pattern on the microstructural evolution of Inconel 625 during selective laser melting," in *2014 Int. Solid Freeform Fabrication Symp.*, 2014, University of Texas at Austin. <http://dx.doi.org/10.26153/tsw/15692>
64. Yuan, B., Guss, G. M., Wilson, A. C., Hau-Riege, S. P., DePond, P. J., McMains, S., Giera, B., "Machine-learning-based monitoring of laser powder bed fusion." *Adv. Mater. Technol.*, 2018, 3(12), 1800136. <https://doi.org/10.1002/admt.201800136>
65. Esmaeilizadeh, R., Ali, U., Keshavarzkhani, A., Mahmoodkhani, Y., Marzbanrad, E., & Toyserkani, E., "On the effect of spatter particles distribution on the quality of Hastelloy X parts made by laser powder-bed fusion additive manufacturing," *J. Manuf. Process.*, 2019, 37, 11–20. <https://doi.org/10.1016/j.jmapro.2018.11.012>

66. Akram, J., Chalavadi, P., Pal, D., & Stucker, B., “*Understanding grain evolution in additive manufacturing through modeling*,” Addit. Manuf., 2018, 21, 255–268.
<https://doi.org/10.1016/j.addma.2018.03.021>
67. Parent, P.-N., Paris, J.-Y., Alexis, J., & Boher, C., “*Influence of the scanning strategy on the microstructure and the tribological behavior of a Ni-based superalloy processed by L-PBF additive manufacturing*,” Wear, 2025, 564, 205671. <https://doi.org/10.1016/j.wear.2024.205671>
68. Wilson, J. M., Piya, C., Shin, Y. C., Zhao, F., & Ramani, K., “*Remanufacturing of turbine blades by laser direct deposition with its energy and environmental impact analysis*,” J. Clean. Prod., 2014, 80, 170–178. <https://doi.org/10.1016/j.jclepro.2014.05.084>
69. Pinkerton, A., Wang, W., & Li, L., “*Component repair using laser direct metal deposition*,” Proc. Inst. Mech. Eng. Part B J. Eng. Manuf., 2008, 222(7), 827–836.
<https://doi.org/10.1243/09544054JEM1008>
70. Kaierle, S., Barroi, A., Noelke, C., Hermsdorf, J., Overmeyer, L., & Haferkamp, H., “*Review on laser deposition welding: From micro to macro*,” Phys. Procedia, 2012, 39, 336–345.
<https://doi.org/10.1016/j.phpro.2012.10.046>
71. Rankouhi, B., Bertsch, K., de Bellefon, G. M., Thevamaran, M., Thoma, D., & Suresh, K., “*Experimental validation and microstructure characterization of topology optimized, additively manufactured SS316L components*,” Mater. Sci. Eng. A, 2020, 776, 139050.
<https://doi.org/10.1016/j.msea.2020.139050>
72. Druzgalski, C., Ashby, A., Guss, G., King, W., Roehling, T., & Matthews, M., “*Process optimization of complex geometries using feed forward control for laser powder bed fusion additive manufacturing*,” Addit. Manuf., 2020, 34, 101169. <https://doi.org/10.1016/j.addma.2020.101169>
73. Asnafi, N., “*Application of Laser-Based Powder Bed Fusion for Direct Metal Tooling*,” Metals, 2021, 11(3), 458. <https://doi.org/10.3390/met11030458>
74. Malekipour, E., & El-Mounayri, H., “*Common defects and contributing parameters in powder bed fusion AM process and their classification for online monitoring and control: a review*,” Int. J. Adv. Manuf. Technol., 2018, 95(1), 527–550.
75. Repossini, G., Laguzza, V., Grasso, M., & Colosimo, B. M., “*On the use of spatter signature for in-situ monitoring of Laser Powder Bed Fusion*,” Addit. Manuf., 2017, 16, 35–48.
<https://doi.org/10.1016/j.addma.2017.05.004>
76. Montazeri, M., & Rao, P., “*Sensor-based build condition monitoring in laser powder bed fusion additive manufacturing process using a spectral graph theoretic approach*,” J. Manuf. Sci. Eng., 2018, 140(9). <https://doi.org/10.1115/1.4040264>
77. Scime, L., & Beuth, J., “*Anomaly detection and classification in a laser powder bed additive manufacturing process using a trained computer vision algorithm*,” Addit. Manuf., 2018, 19, 114–126.
<https://doi.org/10.1016/j.addma.2017.11.009>
78. Whiting, J., Springer, A., & Sciammarella, F., “*Real-time acoustic emission monitoring of powder mass flow rate for directed energy deposition*,” Addit. Manuf., 2018, 23, 312–318.
<https://doi.org/10.1016/j.addma.2018.08.015>

79. Guo, Q., Zhao, C., Escano, L. I., Young, Z., Xiong, L., Fezzaa, K., Chen, L., “*Transient dynamics of powder spattering in laser powder bed fusion additive manufacturing process revealed by in-situ high-speed high-energy x-ray imaging.*” *Acta Mater.*, 2018, 151, 169–180.
<https://doi.org/10.1016/j.actamat.2018.03.036>
80. Young, Z. A., Guo, Q., Parab, N. D., Zhao, C., Qu, M., Escano, L. I., Chen, L., “*Types of spatter and their features and formation mechanisms in laser powder bed fusion additive manufacturing process.*” *Addit. Manuf.*, 2020, 36, 101438. <https://doi.org/10.1016/j.addma.2020.101438>
81. Zhang, Y., Hong, G. S., Ye, D., Zhu, K., & Fuh, J. Y., “*Extraction and evaluation of melt pool, plume and spatter information for powder-bed fusion AM process monitoring,*” *Mater. Des.*, 2018, 156, 458–469. <https://doi.org/10.1016/j.matdes.2018.07.002>
82. Barrett, C., Carradero, C., Harris, E., Rogers, K., MacDonald, E., & Conner, B., “*Statistical analysis of spatter velocity with high-speed stereovision in laser powder bed fusion,*” *Prog. Addit. Manuf.*, 2019, 4(4), 423–430. <https://doi.org/10.1007/s40964-019-00094-6>
83. Yakout, M., Phillips, I., Elbestawi, M., & Fang, Q., “*In-situ monitoring and detection of spatter agglomeration and delamination during laser-based powder bed fusion of Invar 36,*” *Opt. Laser Technol.*, 2021, 136, 106741. <https://doi.org/10.1016/j.optlastec.2020.106741>
84. Barrett, C., Carradero, C., Harris, E., McKnight, J., Walker, J., MacDonald, E., Conner, B., “*Low cost, high speed stereovision for spatter tracking in laser powder bed fusion.*” In: *Proceedings of the 29th Annual International Solid Freeform Fabrication Symposium (SFF)*, 2018, 2122–2134.
<http://dx.doi.org/10.26153/tsw/17206>
85. Chivel, Y., & Smurov, I., “*On-line temperature monitoring in selective laser sintering/melting,*” *Phys. Procedia*, 2010, 5, 515–521. <https://doi.org/10.1016/j.phpro.2010.08.079>
86. Hu, X. D., Kong, F. Z., & Yao, J. H., “*Development of monitoring and control system for laser remanufacturing,*” *Appl. Mech. Mater.*, 2011, 44, 81–85.
<https://doi.org/10.4028/www.scientific.net/AMM.44-47.81>
87. Xing, F., Liu, W., Zhang, K., Shang, X., & Wang, T., “*Intelligent Metal Powder Laser Forming System,*” in *Programming Languages for Manufacturing*, 2006, Springer, 525–535.
https://doi.org/10.1007/0-387-34403-9_72
88. Vasinonta, A., Beuth, J. L., & Ong, R., “*Melt pool size control in thin-walled and bulky parts via process maps,*” *Solid Freeform Fabr. Symp.*, 2001, 432-440 <http://dx.doi.org/10.26153/tsw/3337>
89. Raghavan, A., Wei, H., Palmer, T., & Debroy, T., “*Heat transfer and fluid flow in additive manufacturing,*” *J. Laser Appl.*, 2013, 25(5), 052006. <https://doi.org/10.2351/1.4817788>
90. Khanzadeh, M., Bian, L., Shamsaei, N., & Thompson, S. M., “*Porosity detection of laser based additive manufacturing using melt pool morphology clustering,*” *Solid Freeform Fabr. Symp.*, 2016, 8–10. <https://hdl.handle.net/2152/89688>
91. Caggiano, A., Zhang, J., Alfieri, V., Caiazzo, F., Gao, R., & Teti, R., “*Machine learning-based image processing for on-line defect recognition in additive manufacturing,*” *CIRP Ann.*, 2019, 68(1), 451–454.
<https://doi.org/10.1016/j.cirp.2019.03.021>

92. Masinelli, G., Shevchik, S. A., Pandiyan, V., Quang-Le, T., & Wasmer, K., “*Artificial intelligence for monitoring and control of metal additive manufacturing*,” in *Industrializing Additive Manufacturing: Proc. AMPA2020*, Springer, 2021, 205–220. https://doi.org/10.1007/978-3-030-54334-1_15
93. Cannizzaro, D., Varrella, A. G., Paradiso, S., Sampieri, R., Macii, E., Patti, E. and Di Cataldo, S., “*Image analytics and machine learning for in-situ defects detection in Additive Manufacturing*,” *Proceedings of the Design, Automation & Test in Europe Conference & Exhibition (DATE)*, 2021, 603–608. <https://doi.org/10.23919/DATE51398.2021.9474175>
94. Zhang, B., Liu, S., & Shin, Y. C., “*In-Process monitoring of porosity during laser additive manufacturing process*,” *Addit. Manuf.*, 2019, 28, 497–505. <https://doi.org/10.1016/j.addma.2019.05.030>
95. Hossain, M. S., & Taheri, H., “*In-situ process monitoring for metal additive manufacturing through acoustic techniques using wavelet and convolutional neural network (CNN)*,” *Int. J. Adv. Manuf. Technol.*, 2021, 116(11-12), 3473–3488. <https://doi.org/10.1007/s00170-021-07721-z>
96. Johnson, N. S., Vulimiri, P. S., To, A. C., Zhang, X., Brice, C. A., Kappes, B. B., Stebner, A. P., “*Invited review: Machine learning for materials developments in metals additive manufacturing*,” *Addit. Manuf.*, 2020, 36, 101641. <https://doi.org/10.1016/j.addma.2020.101641>
97. Gobert, C., Reutzel, E. W., Petrich, J., Nassar, A. R., & Phoha, S., “*Application of supervised machine learning for defect detection during metallic powder bed fusion additive manufacturing using high resolution imaging*,” *Addit. Manuf.*, 2018, 21, 517–528. <https://doi.org/10.1016/j.addma.2018.04.005>
98. Li, X., Jia, X., Yang, Q., & Lee, J., “*Quality analysis in metal additive manufacturing with deep learning*,” *J. Intell. Manuf.*, 2020, 31, 2003–2017. <https://doi.org/10.1007/s10845-020-01549-2>
99. Sing, S. L., Kuo, C., Shih, C., Ho, C., & Chua, C. K., “*Perspectives of using machine learning in laser powder bed fusion for metal additive manufacturing*,” *Virtual Phys. Prototyp.*, 2021, 16(3), 372–386. <https://doi.org/10.1080/17452759.2021.1944229>
100. Mohammadi, M. G., Mahmoud, D., & Elbestawi, M., “*On the application of machine learning for defect detection in L-PBF additive manufacturing*,” *Opt. Laser Technol.*, 2021, 143, 107338. <https://doi.org/10.1016/j.optlastec.2021.107338>
101. Angel, N. M., & Basak, A., “*On the fabrication of metallic single crystal turbine blades with a commentary on repair via additive manufacturing*,” *J. Manuf. Mater. Process.*, 2020, 4(4), 101. <https://doi.org/10.3390/jmmp4040101>
102. Menon, N., Mahdi, T. H., & Basak, A., “*Microstructure of IN738LC Fabricated Using Laser Powder Bed Fusion Additive Manufacturing*,” *J. Turbomach.*, 2022, 144(3), 031011. <https://doi.org/10.1115/1.4052404>
103. Menon, N., Sawyer, B. A., Jamieson, C. D., Reutzel, E. W., & Basak, A., “*A Comparison of Microstructure and Microhardness Properties of IN718 Fabricated via Powder- and Wire-Fed Laser-Directed Energy Deposition*,” *Materials*, 2023, 16(3), 1129. <https://doi.org/10.3390/ma16031129>
104. Wang, K., Du, D., Liu, G., Pu, Z., Chang, B., & Ju, J., “*Microstructure and mechanical properties of high chromium nickel-based superalloy fabricated by laser metal deposition*,” *Mater. Sci. Eng. A*, 2020, 780, 139185. <https://doi.org/10.1016/j.msea.2020.139185>

105. Saboori, A., Aversa, A., Marchese, G., Biamino, S., Lombardi, M., & Fino, P., “*Application of directed energy deposition-based additive manufacturing in repair*,” Appl. Sci., 2019, 9(16), 3316. <https://doi.org/10.3390/app9163316>
106. Amato, K. N., Gaytan, S. M., Murr, L. E., Martinez, E., Shindo, P. W., Hernandez, J., Medina, F. J. A. M., “*Microstructures and mechanical behavior of Inconel 718 fabricated by selective laser melting*,” Acta Mater., 2012, 60(5), 2229–2239. <https://doi.org/10.1016/j.actamat.2011.12.032>
107. Costa, L., & Vilar, R., “*Laser powder deposition*,” Rapid Prototyp. J., 2009, 15(4), 264–279. <https://doi.org/10.1108/13552540910979785>
108. Dehghan, A., “*Additive manufacturing as a new technique of fabrication*,” J. 3D Print. Appl., 2018, 1, 3–4. <https://doi.org/10.14302/issn.2831-8846.j3dpa-18-2207>
109. Carter, L. N., Attallah, M. M., & Reed, R. C., “*Laser powder bed fabrication of nickel-base superalloys: influence of parameters; characterisation, quantification and mitigation of cracking*,” Superalloys, 2012, 6, 2826–2834.
110. Li, Y., Liang, X., Yu, Y., Wang, D., & Lin, F., “*Review on additive manufacturing of single-crystal nickel-based superalloys*,” Chin. J. Mech. Eng. Addit. Manuf. Front., 2022, 100019. <https://doi.org/10.1016/j.cjmeam.2022.100019>
111. Xu, J., Ding, Y., Gao, Y., Wang, H., Hu, Y., & Zhang, D., “*Grain refinement and crack inhibition of hard-to-weld Inconel 738 alloy by altering the scanning strategy during selective laser melting*,” Mater. Des., 2021, 209, 109940. <https://doi.org/10.1016/j.matdes.2021.109940>
112. Kalyanasundaram, V., De Luca, A., Wróbel, R., Tang, J., Holdsworth, S. R., Leinenbach, C., Hosseini, E., “*Tensile and creep-rupture response of additively manufactured nickel-based superalloy CM247LC*,” Addit. Manuf. Lett., 2023, 5, 100119. <https://doi.org/10.1016/j.addlet.2022.100119>
113. Yang, J., Li, F., Pan, A., Yang, H., Zhao, C., Huang, W., Zhang, X., “*Microstructure and grain growth direction of SRR99 single-crystal superalloy by selective laser melting*,” J. Alloys Compd., 2019, 808, 151740. <https://doi.org/10.1016/j.jallcom.2019.151740>
114. Song, H. Y., Lam, M. C., Chen, Y., Wu, S., Hodgson, P. D., Wu, X. H., Huang, A. J., “*Towards creep property improvement of selective laser melted Ni-based superalloy IN738LC*,” J. Mater. Sci. Technol., 2022, 112, 301–314. <https://doi.org/10.1016/j.jmst.2021.09.050>
115. Strößner, J., Terock, M., & Glatzel, U., “*Mechanical and microstructural investigation of nickel-based superalloy IN718 manufactured by selective laser melting (SLM)*,” Adv. Eng. Mater., 2015, 17(8), 1099–1105.
116. Amirjan, M., & Khodabandeh, M., “*Direct metal deposition of IN625 on IN738LC superalloy: microstructure and crack analysis*,” Appl. Phys. A, 2021, 127, 1–10. <https://doi.org/10.1016/j.rsurfi.2025.100553>
117. Amirjan, M., & Khodabandeh, M., “*Correlation between processing parameters in direct metal deposition of IN625 nickel-base superalloy*,” J. Mater. Eng. Perform., 2022, 1–14. <https://doi.org/10.1007/s11665-021-06299-7>

118. Jelokhani-Niaraki, M., Mostafa Arab, N. B., Naffakh-Moosavy, H., & Ghoreishi, M., “*The systematic parameter optimization in the Nd: YAG laser beam welding of Inconel 625*,” Int. J. Adv. Manuf. Technol., 2016, 84, 2537–2546. <https://doi.org/10.1007/s00170-015-7833-4>
119. Esmaeilzadeh, M., Qods, F., Arabi, H., & Sadeghi, B. M., “*An investigation on crack growth rate of fatigue and induction heating thermo-mechanical fatigue (TMF) in Hastelloy X superalloy via LEFM, EPFM and integration models*,” Int. J. Fatigue, 2017, 97, 135–149. <https://doi.org/10.1016/j.ijfatigue.2016.12.036>
120. Taheri, N., Naffakh-Moosavy, H., & Ghaini, F. M., “*A new procedure for refurbishment of power plant Superalloy 617 by pulsed Nd: YAG laser process*,” Opt. Laser Technol., 2017, 91, 71–79. <https://doi.org/10.1016/j.optlastec.2016.12.013>
121. Xu, J., Lin, X., Guo, P., Hu, Y., Wen, X., Xue, L., Huang, W., “*The effect of preheating on microstructure and mechanical properties of laser solid forming IN-738LC alloy*,” Mater. Sci. Eng. A, 2017, 691, 71–80. <https://doi.org/10.1016/j.msea.2017.03.046>
122. Wang, X., Keya, T., & Chou, K., “*Build height effect on the Inconel 718 parts fabricated by selective laser melting*,” Procedia Manuf., 2016, 5, 1006–1017. <https://doi.org/10.1016/j.promfg.2016.08.089>
123. Zhang, B., Wang, P., Chew, Y., Wen, Y., Zhang, M., Wang, P., Wei, J., “*Mechanical properties and microstructure evolution of selective laser melting Inconel 718 along building direction and sectional dimension*,” Mater. Sci. Eng. A, 2020, 794, 139941. <https://doi.org/10.1016/j.msea.2020.139941>
124. Donachie, M. J., & Donachie, S. J., Superalloys: A Technical Guide, ASM Int., 2002. <https://doi.org/10.31399/asm.tb.stg2.9781627082679>
125. Dastgerdi, H., Shabani, M. O., & Shajari, Y., “*The effect of cooling rate on the solutionizing of IN718 superalloy produced via selective laser melting (SLM) method*,” J. Environ. Friendly Mater., 2019, 3(1), 17–22.
126. Amirjan, M., Bozorg, M., & Sakiani, H., “*Investigation of microstructure and corrosion behavior of IN718 superalloy fabricated by selective laser melting*,” Mater. Chem. Phys., 2021, 263, 124368. <https://doi.org/10.1016/j.matchemphys.2021.124368>
127. Amirjan, M., & Sakiani, H., “*Heat treated microstructures and properties of additively manufactured IN718 superalloy*,” Phys. Met. Metallogr., 2020, 121, 1382–1392. <https://doi.org/10.1134/S0031918X20140033>
128. Ghaffari, R., & Naffakh-Moosavy, H., “*Investigation of macrostructure, microstructure, and hot cracking susceptibility of laser-welded Inconel-718 superalloy under various post-cold treatment environments*,” CIRP J. Manuf. Sci. Technol., 2022, 37, 110–124. <https://doi.org/10.1016/j.cirpj.2022.01.007>
129. Rezaei, M. A., & Naffakh-moosavy, H., “*Comparison of the effect of pulsed Nd: YAG and continuous wave fiber laser on the microstructure, weld geometry and weldability of Inconel 718 superalloy*,” J. Adv. Mater. Technol., 2019, 7(4), 37–49. <https://doi.org/10.30501/jamt.2019.84346>
130. Naffakh-Moosavy, H., “*Effect of pre-cold treatment on weldability of Inconel 718 superalloy using Nd: YAG pulsed laser*,” Modares Mech. Eng., 2019, 19(2), 327–334.

131. Moosavy, H. N., Aboutalebi, M.-R., Seyedein, S., Goodarzi, M., & Mapelli, C., “Comparative study on dissimilar welding of Inconel 718 and Udimet 500 precipitation strengthened nickel based superalloys,” *Mater. Sci. Technol.*, 2014, 30(3), 339–347.
<https://doi.org/10.1179/1743284713Y.00000000351>
132. Ferreri, N. C., Vogel, S. C., & Knezevic, M., “Determining volume fractions of γ , γ' , γ'' , δ , and MC-carbide phases in Inconel 718 as a function of its processing history using an advanced neutron diffraction procedure,” *Mater. Sci. Eng. A*, 2020, 781, 139228.
<https://doi.org/10.1016/j.msea.2020.139228>
133. Izadi, M., Farzaneh, A., Mohammed, M., Gibson, I., & Rolfe, B., “A review of laser engineered net shaping (LENS) build and process parameters of metallic parts,” *Rapid Prototyp. J.*, 2020.
<https://doi.org/10.1108/RPJ-04-2018-0088>
134. Jiang, R., Mostafaei, A., Wu, Z., Choi, A., Guan, P. W., Chmielus, M., Rollett, A. D., “Effect of heat treatment on microstructural evolution and hardness homogeneity in laser powder bed fusion of alloy 718,” *Addit. Manuf.*, 2020, 35, 101282. <https://doi.org/10.1016/j.addma.2020.101282>
135. Wang, R., Chen, C., Liu, M., Zhao, R., Xu, S., Hu, T., Ren, Z., “Effects of laser scanning speed and building direction on the microstructure and mechanical properties of selective laser melted Inconel 718 superalloy,” *Mater. Today Commun.*, 2022, 30, 103095. <https://doi.org/10.1016/j.mtcomm.2021.103095>
136. Qi, H., Azer, M., & Ritter, A., “Studies of standard heat treatment effects on microstructure and mechanical properties of laser net shape manufactured Inconel 718,” *Metall. Mater. Trans. A*, 2009, 40, 2410–2422. <https://doi.org/10.1007/s11661-009-9949-3>
137. Pröbstle, M., Neumeier, S., Hopfenmüller, J., Freund, L. P., Niendorf, T., Schwarze, D., Göken, M., “Superior creep strength of a nickel-based superalloy produced by selective laser melting,” *Mater. Sci. Eng. A*, 2016, 674, 299–307. <https://doi.org/10.1016/j.msea.2016.07.061>
138. Herzog, D., Seyda, V., Wycisk, E., & Emmelmann, C., “Additive manufacturing of metals,” *Acta Mater.*, 2016, 117, 371–392. <https://doi.org/10.1016/j.actamat.2016.07.019>
139. DebRoy, T., Wei, H. L., Zuback, J. S., Mukherjee, T., Elmer, J. W., Milewski, J. O., Zhang, W., “Additive manufacturing of metallic components—process, structure and properties,” *Prog. Mater. Sci.*, 2018, 92, 112–224. <https://doi.org/10.1016/j.pmatsci.2017.10.001>
140. Hafezi, M., Kermanpur, A., Rezaeian, A., Saeidirad, S., Nikneshan, V., Rabieifar, H., Yousefabad, E. K., “Investigating crack formation in IN738LC Ni-based superalloy fabricated by laser powder-bed fusion process,” *J. Mater. Res. Technol.*, 2024, 29, 1983–2002. <https://doi.org/10.1016/j.jmrt.2024.01.264>
141. Rickenbacher, L., Etter, T., Hövel, S., & Wegener, K., “High temperature material properties of IN738LC processed by selective laser melting (SLM) technology,” *Rapid Prototyp. J.*, 2013.
<https://doi.org/10.1108/13552541311323281>
142. Perevoshchikova, N., Rigaud, J., Sha, Y., Heilmaier, M., Finnin, B., Labelle, E., Wu, X., “Optimisation of selective laser melting parameters for the Ni-based superalloy IN-738 LC using Doehlert’s design,” *Rapid Prototyp. J.*, 2017, 23(5), 881–892. <https://doi.org/10.1108/RPJ-04-2016-0063>
143. Yan, X., Gao, S., Chang, C., Huang, J., Khanlari, K., Dong, D., Liu, M., “Effect of building directions on the surface roughness, microstructure, and tribological properties of selective laser melted

Inconel 625.” J. Mater. Process. Technol., 2021, 288, 116878.
<https://doi.org/10.1016/j.jmatprotec.2020.116878>

144. Attard, B., Cruchley, S., Beetz, C., Megahed, M., Chiu, Y., & Attallah, M., “*Microstructural control during laser powder fusion to create graded microstructure Ni-superalloy components,*” Addit. Manuf., 2020, 36, 101432. <https://doi.org/10.1016/j.addma.2020.101432>

145. Catchpole-Smith, S., Aboulkhair, N., Parry, L., Tuck, C., Ashcroft, I., & Clare, A., “*Fractal scan strategies for selective laser melting of ‘unweldable’ nickel superalloys,*” Addit. Manuf., 2017, 15, 113–122. <https://doi.org/10.1016/j.addma.2017.02.002>

146. Carter, L. N., Martin, C., Withers, P. J., & Attallah, M. M., “*The influence of the laser scan strategy on grain structure and cracking behaviour in SLM powder-bed fabricated nickel superalloy,*” J. Alloys Compd., 2014, 615, 338–347. <https://doi.org/10.1016/j.jallcom.2014.06.172>

147. Lu, Y., Wu, S., Gan, Y., Huang, T., Yang, C., Junjie, L., Lin, J., “*Study on the microstructure, mechanical property and residual stress of SLM Inconel-718 alloy manufactured by differing island scanning strategy.*” Opt. Laser Technol., 2015, 75, 197–206.
<https://doi.org/10.1016/j.optlastec.2015.07.009>

148. Masoomi, M., Thompson, S. M., & Shamsaei, N., “*Quality part production via multi-laser additive manufacturing,*” Manuf. Lett., 2017, 13, 15–20. <https://doi.org/10.1016/j.mfglet.2017.05.003>

149. Balbaa, M., Mekhiel, S., Elbestawi, M., & McIsaac, J., “*On selective laser melting of Inconel 718: Densification, surface roughness, and residual stresses,*” Mater. Des., 2020, 193, 108818.
<https://doi.org/10.1016/j.matdes.2020.108818>

150. Nadammal, N., Cabeza, S., Mishurova, T., Thiede, T., Kromm, A., Seyfert, C., Bruno, G., “*Effect of hatch length on the development of microstructure, texture and residual stresses in selective laser melted superalloy Inconel 718.*” Mater. Des., 2017, 134, 139–150. <https://doi.org/10.1016/j.matdes.2017.08.049>

151. Xia, M., Gu, D., Yu, G., Dai, D., Chen, H., & Shi, Q., “*Influence of hatch spacing on heat and mass transfer, thermodynamics and laser processability during additive manufacturing of Inconel 718 alloy,*” Int. J. Mach. Tools Manuf., 2016, 109, 147–157. <https://doi.org/10.1016/j.ijmachtools.2016.07.010>

152. Saghaian, S. E., Nematollahi, M., Toker, G., Hinojos, A., Moghaddam, N. S., Saedi, S., Karaca, H. E., “*Effect of hatch spacing and laser power on microstructure, texture, and thermomechanical properties of laser powder bed fusion (L-PBF) additively manufactured NiTi.*” Opt. Laser Technol., 2022, 149, 107680. <https://doi.org/10.1016/j.optlastec.2021.107680>

153. Bian, L., Shamsaei, N. and Usher, J. M., Laser-Based Additive Manufacturing of Metal Parts: Modeling, Optimization, and Control of Mechanical Properties. CRC Press, Boca Raton, USA, 2017, 97.
<https://doi.org/10.1201/9781315151441>

154. Benoit, M. J., Mazur, M., Easton, M. A., & Brandt, M., “*Effect of alloy composition and laser powder bed fusion parameters on the defect formation and mechanical properties of Inconel 625,*” Int. J. Adv. Manuf. Technol., 2021, 114, 915–927. <https://doi.org/10.1007/s00170-021-06957-z>

155. Lippold, J. C., Elevated Temperature, Solid-State Cracking in Welds. Cracking Phenomena in Welds IV, eds. Boellinghaus, T., Lippold, J. and Cross, C., Springer, Cham, 2016, 229–265.
https://doi.org/10.1007/978-3-319-28434-7_12

156. Harrison, N. J., *Selective Laser Melting of Nickel Superalloys: solidification, microstructure and material response*, University of Sheffield, 2016.
157. Chaturvedi, M. C., “*Liquation cracking in heat affected zone in Ni superalloy welds*,” Mater. Sci. Forum, 2007, 546, 1163–1170. <https://doi.org/10.4028/www.scientific.net/MSF.546-549.1163>
158. Ciales, L. E., Arisoy, Y. M., Lane, B., Moylan, S., Donmez, A., & Özel, T., “*Laser powder bed fusion of nickel alloy 625: Experimental investigations of effects of process parameters on melt pool size and shape with spatter analysis*,” Int. J. Mach. Tools Manuf., 2017, 121, 22–36. <https://doi.org/10.1016/j.ijmachtools.2017.03.004>
159. Arisoy, Y. M., Ciales, L. E., Ozel, T., Lane, B., Moylan, S., & Donmez, A., “*Influence of scan strategy and process parameters on microstructure and its optimization in additively manufactured nickel alloy 625 via laser powder bed fusion*,” Int. J. Adv. Manuf. Technol., 2017, 90, 1393–1417. <https://doi.org/10.1007/s00170-016-9429-z>
160. Brown, C. U., Jacob, G., Possolo, A., Beauchamp, C., Peltz, M., Donmez, A., “*The effects of laser powder bed fusion process parameters on material hardness and density for nickel alloy 625*,” NIST Adv. Manuf. Ser., 2018, 100–19. <https://doi.org/10.6028/NIST.AMS.100-19>
161. Xu, J., Kontis, P., Peng, R. L., & Moverare, J., “*Modelling of additive manufacturability of nickel-based superalloys for laser powder bed fusion*,” Acta Mater., 2022, 240, 118307. <https://doi.org/10.1016/j.actamat.2022.118307>
162. Martelli, P. A., Sivo, A., Calignano, F., Bassini, E., Biamino, S., & Ugues, D., “*Parameters Optimization and Repeatability Study on Low-Weldable Nickel-Based Superalloy René 80 Processed via Laser Powder-Bed Fusion (L-PBF)*,” Metals, 2023, 13(2), 210. <https://doi.org/10.3390/met13020210>
163. Adegoke, O., Andersson, J., Brodin, H., & Pederson, R., “*Influence of Laser Powder Bed Fusion Process Parameters on Voids, Cracks, and Microhardness of Nickel-Based Superalloy Alloy 247LC*,” Materials, 2020, 13(17), 3770. <https://doi.org/10.3390/ma13173770>
164. Huynh, T., Mehta, A., Graydon, K., Woo, J., Park, S., Hyer, H., Sohn, Y., “*Microstructural development in Inconel 718 nickel-based superalloy additively manufactured by laser powder bed fusion*,” Metallogr. Microstruct. Anal., 2022, 1–20. <https://doi.org/10.1007/s13632-021-00811-0>
165. Yeung, H., Kim, F., Donmez, M., & Neira, J., “*Keyhole pores reduction in laser powder bed fusion additive manufacturing of nickel alloy 625*,” Int. J. Mach. Tools Manuf., 2022, 183, 103957. <https://doi.org/10.1016/j.ijmachtools.2022.103957>
166. Chen, Z., Lu, Y., Luo, F., Zhang, S., Wei, P., Yao, S., Wang, Y., “*Effect of laser scanning speed on the microstructure and mechanical properties of laser-powder-bed-fused K418 nickel-based alloy*,” Materials, 2022, 15(9), 3045. <https://doi.org/10.3390/ma15093045>
167. Acharya, R., Bansal, R., Gambone, J. J., & Das, S., “*A coupled thermal, fluid flow, and solidification model for the processing of single-crystal alloy CMSX-4 through scanning laser epitaxy for turbine engine hot-section component repair (Part I)*,” Metall. Mater. Trans. B, 2014, 45(6), 2247–2261. <https://doi.org/10.1007/s11663-014-0117-9>
168. Paul, S., Liu, J., Strayer, S. T., Zhao, Y., Sridar, S., Klecka, M. A., To, A. C., “*A discrete dendrite dynamics model for epitaxial columnar grain growth in metal additive manufacturing with application to inconel*,” Addit. Manuf., 2020, 36, 101611. <https://doi.org/10.1016/j.addma.2020.101611>

169. Li, Y., Zhang, Z., & Guan, Y., “*Thermodynamics analysis and rapid solidification of laser polished Inconel 718 by selective laser melting*,” Appl. Surf. Sci., 2020, 511, 145423.
<https://doi.org/10.1016/j.apsusc.2020.145423>
170. Yi, J. H., Kang, J. W., Wang, T. J., Wang, X., Hu, Y. Y., Feng, T., Wu, P. Y., “*Effect of laser energy density on the microstructure, mechanical properties, and deformation of Inconel 718 samples fabricated by selective laser melting*,” J. Alloys Compd., 2019, 786, 481–488.
<https://doi.org/10.1016/j.jallcom.2019.01.377>
171. Wan, H., Zhou, Z., Li, C., Chen, G., & Zhang, G., “*Effect of scanning strategy on grain structure and crystallographic texture of Inconel 718 processed by selective laser melting*,” J. Mater. Sci. Technol., 2018, 34(10), 1799–1804. <https://doi.org/10.1016/j.jmst.2018.02.002>
172. Shajari, Y., Razavi, S. H., Seyedraoufi, Z. S., & Samiee, M., “*The effect of time and temperature of solutionizing heat treatment on γ' characterization in a Ni-base superalloy*,” Metallogr. Microstruct. Anal., 2021, 10(4), 441–447. <https://doi.org/10.1007/s13632-021-00760-8>
173. Hashemi, N., Seyedraoufi, Z. S., & Shajari, Y., “*The effect of partial solution heat treatment parameters on microstructure evaluation of IN792 superalloy*,” Metallogr. Microstruct. Anal., 2021, 10, 627–633. <https://doi.org/10.1007/s13632-021-00777-z>
174. Shajari, Y., Razavi, S. H., & Seyedraoufi, Z.-S., “*Comparative study of solution heat treatment of IN738LC superalloy in conventional conditions and salt bath*,” J. Mater. Eng. Perform., 2022, 1–17.
<https://doi.org/10.1007/s11665-021-06344-5>
175. Samiee, M., Shajari, Y., Razavi, S. H., & Seyedraoufi, Z. S., “*Effect of Cryogenic Treatment After Full Solution on Rejuvenation of Exposed IN738LC Gas Turbine Blade*,” Metallogr. Microstruct. Anal., 2022, 1–11. <https://doi.org/10.1007/s13632-022-00917-z>
176. Shajari, Y., Seyedraoufi, Z., Alizadeh, A., Razavi, S., Porhonar, M., & Mirzavand, K., “*Effect of solution temperature of rejuvenation heat treatment on the stability of γ' precipitates in Ni-base superalloy IN738LC during long-term heating*,” Mater. Res. Express, 2019, 6(12), 126571.
<https://doi.org/10.1088/2053-1591/ab54ef>
177. Shajari, Y., Razavi, S. H., & Seyedraoufi, Z. S., “*Effect of Solution Treatment on the Microstructure of γ' Precipitates in the IN738LC Superalloy Before and After Aging*,” Founding Res. J., 2017, 1(2), 99–108. <https://doi.org/10.22034/frj.2018.117722.1022>
178. Arabi, H., Rastegari, S., Mirhosseini, M., & Sadeghi, B., “*Effect of cooling rates from partial solution temperature and aging on γ' precipitation in IN792 superalloy*,” Mater. Sci. Technol., 2013, 29(12), 1513–1517. <https://doi.org/10.1179/1743284713Y.00000000325>
179. Moosavy, H. N., Aboutalebi, M.-R., Seyedein, S. H., Khodabakhshi, M., & Mapelli, C., “*New approach for assessing the weldability of precipitation-strengthened nickel-base superalloys*,” Int. J. Miner. Metall. Mater., 2013, 20, 1183–1191. <https://doi.org/10.1007/s12613-013-0853-x>
180. Basak, A., Acharya, R., & Das, S., “*Additive manufacturing of single-crystal superalloy CMSX-4 through scanning laser epitaxy: computational modeling, experimental process development, and process parameter optimization*,” Metall. Mater. Trans. A, 2016, 47(8), 3845–3859.
<https://doi.org/10.1007/s11661-016-3571-y>

181. Khodabakhshi, A., Mashreghi, A., Shajari, Y., & Razavi, S. H., "Investigation of microstructure properties and quantitative metallography by different etchants in the service-exposed nickel-based superalloy turbine blade," *Trans. Indian Inst. Met.*, 2018, 71(4), 849–859.
<https://doi.org/10.1007/s12666-017-1217-4>
182. Taheri, M., & Kashani-Bozorg, S. F., "Creep behaviors evaluation of IN738 superalloy welded by pulsed Nd:YAG laser through the small punch creep test," *Metallogr. Microstruct. Anal.*, 2021, 10, 199–207. <https://doi.org/10.1007/s13632-021-00729-7>
183. Banerjee, K., Richards, N., & Chaturvedi, M., "Effect of filler alloys on heat-affected zone cracking in preweld heat-treated IN-738 LC gas-tungsten-arc welds," *Metall. Mater. Trans. A*, 2005, 36, 1881–1890. <https://doi.org/10.1007/s11661-005-0051-1>
184. Ojo, O., Richards, N., & Chaturvedi, M., "Study of the fusion zone and heat-affected zone microstructures in tungsten inert gas-welded INCONEL 738LC superalloy," *Metall. Mater. Trans. A*, 2006, 37, 421–433. <https://doi.org/10.1007/s11661-006-0013-2>
185. Osoba, L., & Amuda, M., "Tracking heat-affected zone cracking susceptibility in standard and modified heat treated IN 738 superalloy welds," *High Performance and Optimum Design of Structures and Materials*, 2014, 137, 37. <http://dx.doi.org/10.2495/HPSM140041>
186. Speicher, M., Scheck, R., & Maile, K., "Influence of Different Etchants on the Representation of Microstructures in Nickel Alloys," *Pract. Metallogr.*, 2016, 53(4), 206–220.
<https://doi.org/10.3139/147.110385>
187. Wang, W., Chen, Z., Lu, W., Meng, F., & Zhao, T., "Heat treatment for selective laser melting of Inconel 718 alloy with simultaneously enhanced tensile strength and fatigue properties," *J. Alloys Compd.*, 2022, 913, 165171. <https://doi.org/10.1016/j.jallcom.2022.165171>
188. Gao, Y., Zhang, D., Cao, M., Chen, R., Feng, Z., Poprawe, R., Ziegler, S., "Effect of δ phase on high temperature mechanical performances of Inconel 718 fabricated with SLM process," *Mater. Sci. Eng. A*, 2019, 767, 138327. <https://doi.org/10.1016/j.msea.2019.138327>
189. Teng, Q., Li, S., Wei, Q., & Shi, Y., "Investigation on the influence of heat treatment on Inconel 718 fabricated by selective laser melting: Microstructure and high temperature tensile property," *J. Manuf. Process.*, 2021, 61, 35–45. <https://doi.org/10.1016/j.jmapro.2020.11.002>
190. He, S., Guo, S., & Xu, Y., "Anisotropic Stress Rupture Properties-Microstructure Relationships in SLM Inconel 718 Alloy," *Metall. Mater. Trans. A*, 2023, 54(5), 1776–1791.
<https://doi.org/10.1007/s11661-022-06872-2>
191. Trosch, T., Strößner, J., Völkl, R., & Glatzel, U., "Microstructure and mechanical properties of selective laser melted Inconel 718 compared to forging and casting," *Mater. Lett.*, 2016, 164, 428–431.
<https://doi.org/10.1016/j.matlet.2015.10.136>
192. Soni, H., Gor, M., Rajput, G. S., & Sahlot, P., "A comprehensive review on effect of process parameters and heat treatment on tensile strength of additively manufactured Inconel-625," *Mater. Today: Proc.*, 2021, 47, 4866–4871. <https://doi.org/10.1016/j.matpr.2021.06.126>
193. Hu, X.-A., Zhao, G.-L., Liu, F.-C., & Liu, W.-X., "Microstructure and mechanical behavior of Inconel 625 alloy processed by selective laser melting at high temperature up to 1000 °C," *Rare Metals*, 2020, 39, 1181–1189. <https://doi.org/10.1007/s12598-019-01321-3>

194. Yi, F., Zhou, Q., Wang, C., Yan, Z., & Liu, B., “*Effect of powder reuse on powder characteristics and properties of Inconel 718 parts produced by selective laser melting*,” J. Mater. Res. Technol., 2021, 13, 524–533. <https://doi.org/10.1016/j.jmrt.2021.04.091>
195. Li, Y., Dlouhý, J., Vavřík, J., Džugan, J., Konopík, P., Krajňák, T., Veselý, J., “*Investigation of short-term creep properties of a coarse-grained Inconel 718 fabricated by directed energy deposition compared to traditional Inconel 718*,” Mater. Sci. Eng. A, 2022, 844, 143143. <https://doi.org/10.1016/j.msea.2022.143143>
196. Ma, T., Zhang, G.-P., Tan, P., & Zhang, B., “*Effects of homogenization temperature on creep performance of laser powder bed fusion-fabricated Inconel 718 at 650 °C*,” Mater. Sci. Eng. A, 2022, 853, 143794. <https://doi.org/10.1016/j.msea.2022.143794>
197. Shi, J. J., Zhou, Z. Q., Xu, K., Zhou, G. Y., Zhou, Z. J., Li, C. P., Cao, G. H., “*Effect of heat treatment on microstructure and small punch creep property of selective laser melted Inconel 718 alloy*,” Mater. Sci. Eng. A, 2022, 853, 143748. <https://doi.org/10.1016/j.msea.2022.143748>
198. Wang, L. Y., Wang, Y. C., Zhou, Z. J., Wan, H. Y., Li, C. P., Chen, G. F., Zhang, G. P., “*Small punch creep performance of heterogeneous microstructure dominated Inconel 718 fabricated by selective laser melting*,” Mater. Des., 2020, 195, 109042. <https://doi.org/10.1016/j.matdes.2020.109042>
199. Wang, L., Zhou, Z., Li, C., Chen, G., & Zhang, G., “*Comparative investigation of small punch creep resistance of Inconel 718 fabricated by selective laser melting*,” Mater. Sci. Eng. A, 2019, 745, 31–38. <https://doi.org/10.1016/j.msea.2018.12.083>
200. Xu, Z., Cao, L., Zhu, Q., Guo, C., Li, X., Hu, X., Yu, Z., “*Creep property of Inconel 718 superalloy produced by selective laser melting compared to forging*,” Mater. Sci. Eng. A, 2020, 794, 139947. <https://doi.org/10.1016/j.msea.2020.139947>
201. Popovich, V., Borisov, E., Heurtebise, V., Riemslog, T., Popovich, A., & Sufiarov, V. S., “*Creep and thermomechanical fatigue of functionally graded Inconel 718 produced by additive manufacturing*,” in TMS 2018 147th Annual Meeting & Exhibition Supplemental Proceedings, Springer, 2018, 85–97. https://doi.org/10.1007/978-3-319-72526-0_9
202. Shi, J. J., Li, X., Zhang, Z. X., Cao, G. H., Russell, A. M., Zhou, Z. J., Chen, G. F., “*Study on the microstructure and creep behavior of Inconel 718 superalloy fabricated by selective laser melting*,” Mater. Sci. Eng. A, 2019, 765, 138282. <https://doi.org/10.1016/j.msea.2019.138282>
203. Shi, J. J., Zhou, S. A., Chen, H. H., Cao, G. H., Russell, A. M., Zhou, Z. J., Chen, G. F., “*Microstructure and creep anisotropy of Inconel 718 alloy processed by selective laser melting*,” Mater. Sci. Eng. A, 2021, 805, 140583. <https://doi.org/10.1016/j.msea.2020.140583>
204. Karabulut, Y., Tascioglu, E., & Kaynak, Y., “*Heat treatment temperature-induced microstructure, microhardness and wear resistance of Inconel 718 produced by selective laser melting additive manufacturing*,” Optik, 2021, 227, 163907. <https://doi.org/10.1016/j.ijleo.2019.163907>
205. Yang, H., Yang, J., Huang, W., Wang, Z., & Zeng, X., “*The printability, microstructure, crystallographic features and microhardness of selective laser melted Inconel 718 thin wall*,” Mater. Des., 2018, 156, 407–418. <https://doi.org/10.1016/j.matdes.2018.07.007>

206. Shajari, Y., Seyedraoufi, Z. S., Razavi, S. H., Nasri, M., & Khiabani, A., “*Effect of Remelting and Standard Heat Treatment on Microstructure and Mechanical Properties of IN738LC Superalloy*,” *Founding Res. J.*, 2020, 4(2), 99–109. <https://doi.org/10.22034/frj.2020.238339.1122>
207. Flemings, M. C., “*Solidification processing*,” *Metall. Mater. Trans. B*, 1974, 5, 2121–2134. <https://doi.org/10.1007/BF02643923>
208. Yang, C., Hu, R., Liu, X., Wang, Y., Bai, J., & Ma, R., “*Microstructural evolution and high-temperature strengthening mechanisms of the IN 738LC superalloy prepared by selective laser melting*,” *J. Mater. Res. Technol.*, 2024, 29, 5304–5316. <https://doi.org/10.1016/j.jmrt.2024.02.219>
209. Javidrad, H., Aydin, H., Karakaş, B., Alptekin, S., Kahraman, A. S., & Koc, B., “*Process parameter optimization for laser powder directed energy deposition of Inconel 738LC*,” *Opt. Laser Technol.*, 2024, 176, 110940. <https://doi.org/10.1016/j.optlastec.2024.110940>
210. Lu, X., Zhang, G., Chiumenti, M., Cervera, M., Wang, Z., Yao, B., Lin, X., “*Additive manufacturing of crack-free large IN738LC parts through tailored substrate designs*,” *Thin-Walled Struct.*, 2025, 112979. <https://doi.org/10.1016/j.tws.2025.112979>
211. Liu, Z., Zhou, Q., Liang, X., Wang, X., Li, G., Vanmeensel, K., Xie, J., “*Alloy design for laser powder bed fusion additive manufacturing: A critical review*,” *Int. J. Extrem. Manuf.*, 2024, 6(2), 022002. <https://doi.org/10.1088/2631-7990/ad1657>
212. Song, W., Yang, J., Liang, J., Lu, N., Zhou, Y., Sun, X., Li, J., “*A new approach to design advanced superalloys for additive manufacturing*,” *Addit. Manuf.*, 2024, 84, 104098. <https://doi.org/10.1016/j.addma.2024.104098>
213. Gilakjani, R. S., Razavi, S. H., & Seifollahi, M., “*The Effect of Niobium Addition on the Microstructure and Tensile Properties of Iron-Nickel Base A286 Superalloy*,” *Iran. J. Mater. Sci. Eng.*, 2021, 18(1). <https://doi.org/10.22068/ijmse.18.1.7>
214. Ghaemifar, S., & Mirzadeh, H., “*Unveiling the Effect of Annealing Temperature on the Phase Transformations of Inconel 718 Super alloy Manufactured by Additive Manufacturing*,” *Iran. J. Mater. Sci. Eng.*, 2023, 20(4). <https://doi.org/10.22068/ijmse.3304>
215. Riazi, A., Razavi, S. H., Khavandi, A., Amirjan, M., Shabani, M. O., & Davarzani, H., “*A new approach to the reasons for dependency of defects formation to the process parameters in laser powder bed fusion of IN625 on the IN738LC substrate*,” *J. Adv. Joining Process.*, 2025, 11, 100273. <https://doi.org/10.1016/j.jajp.2024.100273>
216. Riazi, A., Razavi, S. H., Khavandi, A., Amirjan, M., Shabani, M. O., & Davarzani, H., “*Influence of Process Parameters on Melt Pool Morphology and Elemental Diffusion in LPBF of IN625 on IN738 Substrate*,” *Results Surf. Interfaces*, 2025, 100553. <https://doi.org/10.1016/j.rsufri.2025.100553>

Glossary

AM: Additive Manufacturing

LBAM: Laser-Based Additive Manufacturing

LPBF: Laser Powder Bed Fusion

NBSAs: Nickel-Based Superalloys

HAZ: Heat-Affected Zone

SLM: Selective Laser Melting

DLD: Direct Laser Deposition

DED: Directed Energy Deposition

EBPBF: Electron Beam Powder Bed Fusion

HIP: Hot Isostatic Pressing